Title: Tuft cell-derived acetylcholine regulates epithelial fluid secretion

Authors: Tyler E. Billipp[1], Connie Fung[2], Lily M. Webeck[1], Derek B. Sargent[1], Matthew B. Gologorsky[2,3], Margaret M. McDaniel[1], Darshan N. Kasal[1], John W. McGinty[1], Kaitlyn A. Barrow[4], Lucille M. Rich[4], Alessio Barilli[5], Mark Sabat[6†], Jason S. Debley[4,7], Richard Myers[6], Michael R. Howitt[2,3], Jakob von Moltke[1*]

Affiliations:

1 Department of Immunology, University of Washington School of Medicine, Seattle, Washington, USA.

2 Department of Pathology, Stanford University School of Medicine, Stanford, CA 94305, USA

3 Department of Microbiology and Immunology, Stanford University School of Medicine, Stanford, CA 94305, USA

4 Center for Immunity and Immunotherapies, Seattle Children's Research Institute, Seattle, Washington, USA

5 Aptuit, an Evotec Company, Verona, Italy

6 Takeda Pharmaceuticals, San Diego, California, USA

7 Department of Pediatrics, Division of Pulmonary and Sleep Medicine, Seattle Children's Hospital, University of Washington, Seattle, WA, USA

* Correspondence and lead contact: jmoltke@uw.edu

† Now at Atomwise, San Francisco, California, USA

Abstract:

Tuft cells are solitary chemosensory epithelial cells that can sense lumenal stimuli at mucosal barriers and secrete effector molecules to regulate the physiology and immune state of their surrounding tissue. In the small intestine, tuft cells detect parasitic worms (helminths) and microbe-derived succinate, and signal to immune cells to trigger a Type 2 immune response that leads to extensive epithelial remodeling spanning several days. Acetylcholine (ACh) from airway tuft cells has been shown to stimulate acute changes in breathing and mucocilliary clearance, but its function in the intestine is unknown. Here we show that tuft cell chemosensing in the intestine leads to release of ACh, but that this does not contribute to immune cell activation or associated tissue remodeling. Instead, tuft cell-derived ACh triggers immediate fluid secretion from neighboring epithelial cells into the intestinal lumen. This tuft cell-regulated fluid secretion is amplified during Type 2 inflammation, and helminth clearance is delayed in mice lacking tuft cell ACh. The coupling of the chemosensory function of tuft cells with fluid secretion creates an epithelium-intrinsic response unit that effects a physiological change within seconds of activation. This response mechanism is shared by tuft cells across tissues, and serves to regulate the epithelial secretion that is both a hallmark of Type 2 immunity and an essential component of homeostatic maintenance at mucosal barriers.

63 **Introduction:**

64 The physiologic function and immune defense of mucosal tissues require fluid
65 secretion, and epithelial cells employ multiple independent mechanisms to regulate this
66 process. For example, cyclic AMP (cAMP) induces apical chloride (Cl^-) secretion from
67 epithelial cells through cystic fibrosis transmembrane conductance regulator (CFTR).[1]
68 The resulting ionic gradient draws Na^+ and then water out of the tissue and into the
69 lumen, where it hydrates mucus and can contribute to epithelial "flushing".[2,3] Loss-of-
70 function mutations in CFTR cause cystic fibrosis, a disease characterized by viscous
71 mucus, reduced lung function, and bacterial overgrowth.[1] Epithelial Cl^-/water secretion
72 can also occur via calcium-dependent ion channels, with muscarinic acetylcholine
73 receptors (mAChR) in the basolateral membrane often inducing the necessary
74 intracellular calcium flux.[2] Acetylcholine (ACh) is a canonical neurotransmitter
75 synthesized by the enzyme choline acetyltransferase (*Chat*). Neurons innervating
76 mucosal barriers can induce ACh-dependent fluid secretion, but non-neuronal sources
77 of ACh have now been widely reported in other contexts.[3–7]

78 Among epithelial cells, tuft cells are the dominant source of ACh.[8,9] Found across
79 mucosal tissues, they are a lineage of chemosensory cells that monitor the lumenal
80 microenvironment and release effectors to regulate the mucosa. *Chat* expression is part
81 of a transcriptional signature shared by all murine tuft cells[10,11] and ChAT protein has
82 been detected in human tuft cells in the intestine and airways.[12,13] The function of tuft
83 cell-derived ACh has also been studied in several tissues. For example, tuft cells in the
84 nasal epithelium sense bitter and bacteria-derived ligands[14] and secrete ACh, which
85 signals on neurons to induce neurogenic inflammation.[15] Tracheal tuft cells activate
86 nicotinic ACh receptors (nAChRs) to cause a brief cessation in breathing[16] and
87 mAChRs on neighboring epithelial cells to increase ciliary beat frequency[8,17] in
88 response to similar ligands. Likewise, tuft cells in the urethra use ACh to activate
89 neurons and regulate urine release.[18,19] However, the function of tuft cell-derived ACh in
90 the intestine is unknown, nor has a link between tuft cells and fluid secretion been
91 tested.

92 Small intestinal (SI) tuft cells play a critical role in the initiation of "Type 2"
93 immune responses to helminth infection and colonization by *Tritrichomonas sp.*

94 protists.[20,21,22] Tuft cells express SUCNR1, the receptor for extracellular succinate,
95 which *Tritrichomonas sp.* and the microbiota secrete as a metabolite.[11,23,24] SUCNR1
96 signaling causes intracellular Ca^{2+} flux that opens the cation channel TRPM5. The
97 resulting Na^{+} influx depolarizes the tuft cell and likely regulates secretion of most tuft
98 cell effector molecules.[25,26] *Sucnr1*$^{-/-}$ mice fail to detect *Tritrichomonas sp.* colonization,
99 but the immune response to helminth infection is unaffected.[11,24] Nonetheless, sensing
100 of both helminths and protists is severely attenuated in *Trpm5*$^{-/-}$ mice or *Pou2f3*$^{-/-}$ mice
101 that lack tuft cells entirely.[11,20,22]

102 Once activated by lumenal signals, tuft cells produce IL-25 and, in some cases,
103 leukotriene C4 (LTC_4) to activate resident group 2 innate lymphoid cells (ILC2s) in the
104 underlying *lamina propria* (LP).[21,27] ILC2s secrete canonical Type 2 cytokines, including
105 IL-13, that collectively recruit Type 2 immune cells and coordinate intestinal remodeling.
106 Among its many targets, IL-13 produced by ILC2s signals on undifferentiated epithelial
107 cells to bias differentiation towards mucus-producing goblet cells and tuft cells.[20,21,28,29]
108 Given the 3-5 day turnover of the intestinal epithelium, this feed-forward process, known
109 as the tuft-ILC2 circuit, results in dramatic hyperplasia of both goblet cells and tuft cells,
110 the latter of which increase 10-fold.[20,21,22]

111 The Type 2 effector functions that clear worms from the intestine,[30,31] collectively
112 referred to as “weep and sweep,” require the coordination of multiple signals. In addition
113 to increasing the number of tuft and goblet cells, IL-13 upregulates production of mucus
114 and anti-helminthic/microbial peptides in the epithelium,[32,33,34] increases fluid
115 secretion,[35] and increases expression of mAChRs on smooth muscle,[36,37,38] but actual
116 secretion (“weep”) and muscle contraction (“sweep”) generally require additional
117 signals. ACh is one molecule that can acutely activate both weep and sweep,[38] and
118 mAChRs are required for helminth clearance.[39,40] Conversely, helminths secrete ACh
119 esterases (AChE), likely in an attempt to inhibit weep and sweep responses.[41,42,43] The
120 sources of ACh in Type 2 immunity, however, are not defined.

121 By sensing lumenal signals and activating ILC2s, tuft cells serve as sentinels for
122 intestinal Type 2 immunity, but the fact that many more tuft cells are generated after the
123 agonist has been detected suggests an additional effector function for these cells. Here
124 we describe such an effector function, which is independent of ILC2s. We show that in

125 response to sensing of succinate or direct activation of TRPM5, tuft cells secrete ACh to
126 induce epithelial fluid secretion in the intestine and airways. During Type 2 tissue
127 remodeling, *Chat*+ tuft cells increase in number, enhancing the fluid secretion response.
128 Upon helminth infection, mice with *Chat*-deficient tuft cells experience delayed helminth
129 clearance despite normal tuft-ILC2 circuit activation. We conclude that tuft cell-derived
130 ACh regulates epithelial fluid secretion, and that this effector function can contribute to
131 Type 2 immune responses during helminth infection.
132
133 **Results:**
134 ***SI tuft cells express Chat in a proximal to distal gradient***
135 Neuronal *Chat* is important for intestinal function, but the role of *Chat* in intestinal
136 tuft cells has not been studied. To assess *Chat* expression by tuft cells in the SI at
137 single cell resolution, we employed *Chat-GFP* transgenic reporter mice. Immunolabeling
138 for GFP colocalized with the tuft cell marker DCLK1 in both the proximal SI (pSI; first 5-
139 10 cm) and distal SI (dSI; last 5-10 cm) (Fig. 1A). By flow cytometry, >99% of GFP+
140 epithelial cells stained for the tuft cell-specific *Il25-RFP* reporter (Fig. 1B). However, not
141 all tuft cells were GFP+ (Fig. S1A), and we observed a gradient in the frequency of
142 GFP+ tuft cells that increased from 40% of all tuft cells in the pSI to 80% in the dSI (Fig.
143 1C-D). The discovery of GFP-negative tuft cells was unexpected, as the *Chat* reporter
144 marks nearly 100% of tuft cells in other tissues.[8] To validate our findings, we crossed
145 *Chat*-Cre mice, in which Cre is expressed from the endogenous *Chat* locus, to
146 *Rosa26::STOP*$^{fl/fl}$*::CAG-tdTomato* (Ai9) mice for lineage tracing. Using CD24 and
147 Siglec-F to identify tuft cells, we again observed both reporter-positive and -negative tuft
148 cells, with an increased frequency of reporter-positive tuft cells in the distal compared to
149 the proximal SI (Fig. S1B).

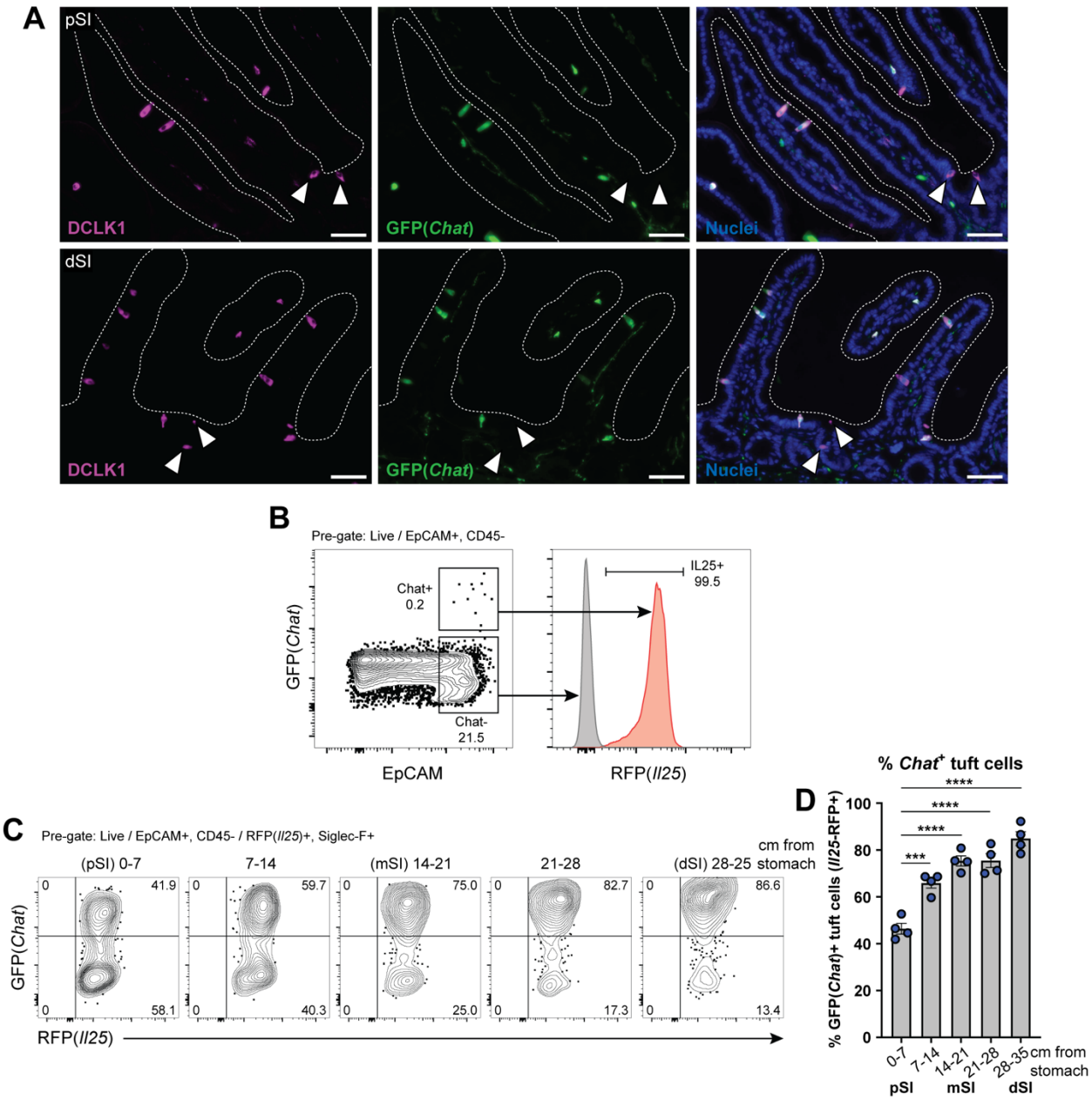

Figure 1: SI tuft cells express *Chat* in a proximal to distal gradient. (**A**) Representative images of GFP(*Chat*) expression (green) by DCLK1+ tuft cells (magenta) in the proximal SI (pSI) and distal SI (dSI) by immunofluorescence. White arrows indicate GFP(*Chat*)- tuft cells. Nuclei stained with DAPI (blue). Scale bars: 50 µm (**B**) GFP+ epithelial cells (EpCAM+) are RFP(*Il25*)+ tuft cells. (**C** and **D**) (C) Representative flow cytometry and (D) quantification of the percentage of GFP+ tuft cells by sequential 7 cm section across the length of the SI. In D, each symbol represents an individual mouse (columns represent different tissues from same mouse) from three pooled experiments. *p < 0.05, **p < 0.01, ***p < 0.001 by one way ANOVA with Tukey's multiple comparisons test (D). mSI, medial SI. Graphs depict mean +/- SEM. Also see Figure S1.

161 Given the binary nature of *Chat-GFP* expression in SI tuft cells, we hypothesized
162 that *Chat* might mark transcriptionally distinct tuft cell subsets. We therefore sorted
163 GFP+ and GFP- tuft cells, performed bulk RNA sequencing, and identified differentially
164 expressed genes (DEGs) (Fig. S1C, Table S1, Data File S1). Surprisingly, despite the
165 binary nature of GFP expression, *Chat* was downregulated only 2.8-fold (FDR = .0009)
166 in GFP- cells, suggesting translation is regulated via untranslated regions of the
167 endogenous *Chat* transcript that are retained in the transgene (Fig. S1C). More broadly,
168 even with a lenient fold-change (FC) cutoff of 2 (FDR <.01), there were only 105 DEGs.
169 None of the downregulated genes were part of the SI tuft cell signature,[44] but *Sucnr1*
170 (FC = 3.3, FDR = .0007) and the downstream G alpha subunit *Gnat3* (FC = 4.9, FDR =
171 .0001) were upregulated in GFP+ cells (Fig S1C, Table S1). Comparing *Chat*+ tuft cells
172 to previously reported intestinal tuft cell subsets "Tuft-1" and "Tuft-2",[9] we found greater
173 enrichment for Tuft-2 genes (Fig. S1D), but the best match was with a dSI tuft cell
174 signature we generated by sorting tuft cells from the proximal and distal 5 cm of
175 unmanipulated intestines (Fig. S1D-E, Table S2, Data File S2). This signature similarly
176 includes *Sucnr1* and *Gnat3,* and we hypothesize that transcriptional differences
177 between GFP+ and GFP- cells resulted mostly from a distal bias among sorted GFP+
178 cells, consistent with the gradient we observed (Fig. 1D).
179 We also considered the possibility that *Chat*- cells were an immature stage
180 before *Chat*+ cells, but while GFP+ cells predominated in the villi and GFP- cells in the
181 crypts, there were still GFP+ cells in the crypts (Fig. S1F) and GFP- cells at the villus
182 tips (Fig. S1G), making a developmental relationship unlikely. Both IL4ra-dependent
183 and IL4ra-independent tuft cells have been identified in the SI,[45] but we found many
184 *Chat-GFP*+ tuft cells in the SI of *Il4ra*$^{-/-}$ mice, suggesting *Chat* expression is not
185 exclusive to IL-13-induced tuft cells (Fig. S1H). The mechanisms regulating *Chat*
186 expression in tuft cells therefore remain unknown.

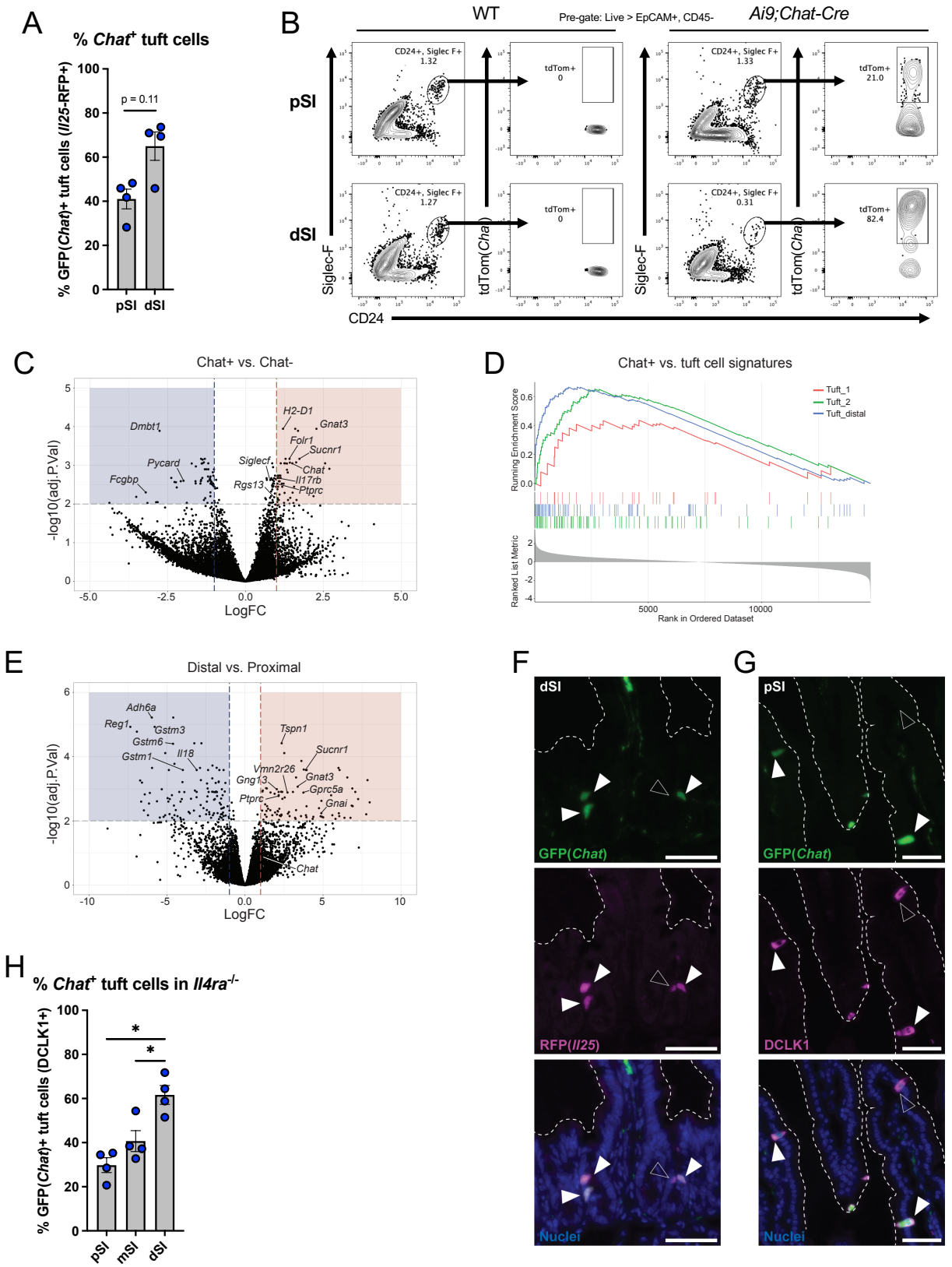
A
% Chat+ tuft cells
% GFP(Chat)+ tuft cells (Il25-RFP+)
p = 0.11
pSI
dSI
B
WT
Pre-gate: Live > EpCAM+, CD45-
Ai9;Chat-Cre
pSI
dSI
CD24+, Siglec F+
1.32
tdTom+
0
1.33
21.0
1.27
0
0.31
82.4
Siglec-F
tdTom(Chat)
CD24
C
Chat+ vs. Chat-
-log10(adj.P.Val)
LogFC
Dmbt1
Pycard
Fcgbp
H2-D1
Gnat3
Folr1
Sucnr1
Siglecf
Chat
Rgs13
Il17rb
Ptprc
D
Chat+ vs. tuft cell signatures
Tuft_1
Tuft_2
Tuft_distal
Running Enrichment Score
Ranked List Metric
Rank in Ordered Dataset
E
Distal vs. Proximal
Adh6a
Reg1
Gstm3
Gstm6
Gstm1
Il18
Tspn1
Sucnr1
Vmn2r26
Gng13
Gnat3
Gprc5a
Ptprc
Gnai
Chat
F
dSI
GFP(Chat)
RFP(Il25)
Nuclei
G
pSI
GFP(Chat)
DCLK1
Nuclei
H
% Chat+ tuft cells in Il4ra-/-
% GFP(Chat)+ tuft cells (DCLK1+)
pSI
mSI
dSI

188 **Supplemental Figure 1:** (**A**) Quantification of GFP+ tuft cells (RFP+) from pSI and dSI of *Chat-*
189 *GFP*;*Il25*$^{RFP/+}$ mice by immunofluorescence (IF). (**B**) Representative flow cytometry of traced tdTom+ tuft
190 cells (CD24+, Siglec-F+) from pSI and dSI of wild-type (WT) and *Ai9;Chat-Cre* mice. (**C**) Volcano plot
191 showing log2FC of genes expressed in *Chat*+ tuft cells (n=4) versus *Chat*- tuft cells (n=3) sorted from
192 whole SI of *Chat-GFP*;*Il25*$^{RFP/+}$ mice. (**D**) Gene set enrichment analysis comparing *Chat*+ tuft cell gene
193 expression to Tuft-1 and Tuft-2 consensus gene signatures and the dSI tuft cell signature from (**E**)
194 Volcano plot showing log2FC of genes expressed in tuft cells sorted from the dSI (n=4) versus tuft cells
195 sorted from the pSI (n=4) of B6 mice. (**F**) Representative immunofluorescence image showing GFP+
196 (green) tuft cells (RFP+, magenta) in the SI crypt (solid white arrows), next to one GFP- tuft cell (open
197 white arrow). Nuclei stained with DAPI (blue). Scale bars: 50 µm. (**G**) Representative
198 immunofluorescence image showing a GFP- (green) tuft cell (DCLK1+, magenta) at the villus tip (open
199 white arrow), past other GFP+ tuft cells (solid white arrows). Nuclei stained with DAPI (blue). Scale bars:
200 50 µm. (**H**) Quantification of GFP(*Chat*)+ tuft cells (DCLK1+) from denoted tissues of *Il4ra*$^{-/-}$*;Chat-GFP*
201 mice by immunofluorescence. In the graphs, each symbol represents an individual mouse (columns
202 represent different tissues from same mouse) from two pooled experiments. *$p < 0.05$, **$p < 0.01$, ***$p <$
203 0.001 by Mann-Whitney test (A) or one way ANOVA with Tukey's multiple comparisons test (G). mSI,
204 medial SI. Graphs depict mean +/- SEM.
205

206 ***ACh from tuft cells induces fluid secretion from the SI epithelium***

207 ACh rapidly induces fluid, mucus, and antimicrobial peptide secretion when it
208 binds muscarinic ACh receptors (mAChRs) on SI epithelial cells.[4,46,47,48] Classically,
209 enteric neurons are considered the primary source of ACh that regulates SI
210 secretion,[4,49,50] but we hypothesized that tuft cells could link lumenal chemosensing to
211 epithelial secretion via basolateral release of ACh.

212 To make sensitive, real-time measurements of SI epithelial electrophysiology, we
213 employed Ussing chambers,[51] which have been used to measure ACh-induced
214 epithelial ion flux.[52] Two chambers containing physiologic buffer are separated by a
215 piece of SI epithelium and the voltage across the epithelium is clamped. When
216 negatively charged ions (e.g. Cl^-) are secreted into the lumenal chamber, current is
217 injected into the basolateral chamber to restore the voltage (Fig. 2A). This "short-circuit"
218 current, or Isc, is directly proportional to ion flux.[51]

219 To test whether tuft cells regulate ion flux, we mounted SI tissue from
220 unmanipulated mice in the Ussing chamber and stimulated with Na_2-succinate
221 (succinate), since it is the best-defined ligand for SI tuft cells.[11,23,24] When we stimulated

222 the lumenal side of the SI tissue with 10 mM succinate, we recorded a rapid increase in
223 the Isc that lasted several minutes before returning close to baseline (Fig. 2B). We
224 quantified this response by measuring the change in Isc from the baseline before
225 stimulation to its peak, known as the delta Isc (ΔIsc; see Fig. 2B inset). To control for
226 the addition of sodium, we tested NaCl at an equimolar concentration of sodium (20
227 mM). NaCl was sufficient to increase the Isc, but the response was
228 significantly smaller than the succinate response and failed to return to baseline. The
229 succinate response, on the other hand, had similar kinetics to the response elicited by
230 the ACh mimic carbachol (CCh), given basolaterally to maximally stimulate mAChRs
231 (Fig. 2B). The succinate response was greatly diminished in SI from *Sucnr1*$^{-/-}$ mice,
232 though a residual, likely sodium-dependent increase remained (Fig. S2A). To avoid the
233 sodium response, we used the synthetic SUCNR1 agonist cis-epoxysuccinic acid
234 (cESA),[53] which stimulated an Isc response comparable to succinate, but that was
235 entirely *Sucnr1*-dependent (Fig. S2A). We used cESA in place of succinate for most of
236 the subsequent Ussing experiments.
237 To further characterize the succinate/cESA Isc response, we began by testing
238 the role of epithelial polarity. cESA induced ion flux when given lumenally, but not
239 basolaterally, consistent with lumenal restriction of SUCNR1 in tuft cells (Fig. S2B).
240 Conversely, CCh stimulated ion flux when given basolaterally, but not lumenally,
241 consistent with basolateral restriction of mAChRs on intestinal epithelial cells (IECs).[4]
242 Since the Isc represents net ion flux across the epithelium, the increased Isc response
243 to succinate could be due to either increased lumenal secretion of negatively charged
244 anions (e.g. Cl^-, $HCO3^-$) or increased absorption of positively charged cations (e.g. Na^+,
245 K^+) from the lumen.[4] To test the contribution of Cl^- ions selectively, we replaced Cl^- with
246 gluconate, which cannot cross the epithelium,[51,54] and found that both the cESA and
247 CCh responses were abrogated (Fig. 2C). Bumetanide, an inhibitor of the basolateral
248 chloride transporter NKCC1 that is required for sustained Cl^- secretion,[1] likewise
249 decreased the response to cESA (Fig. S2C).

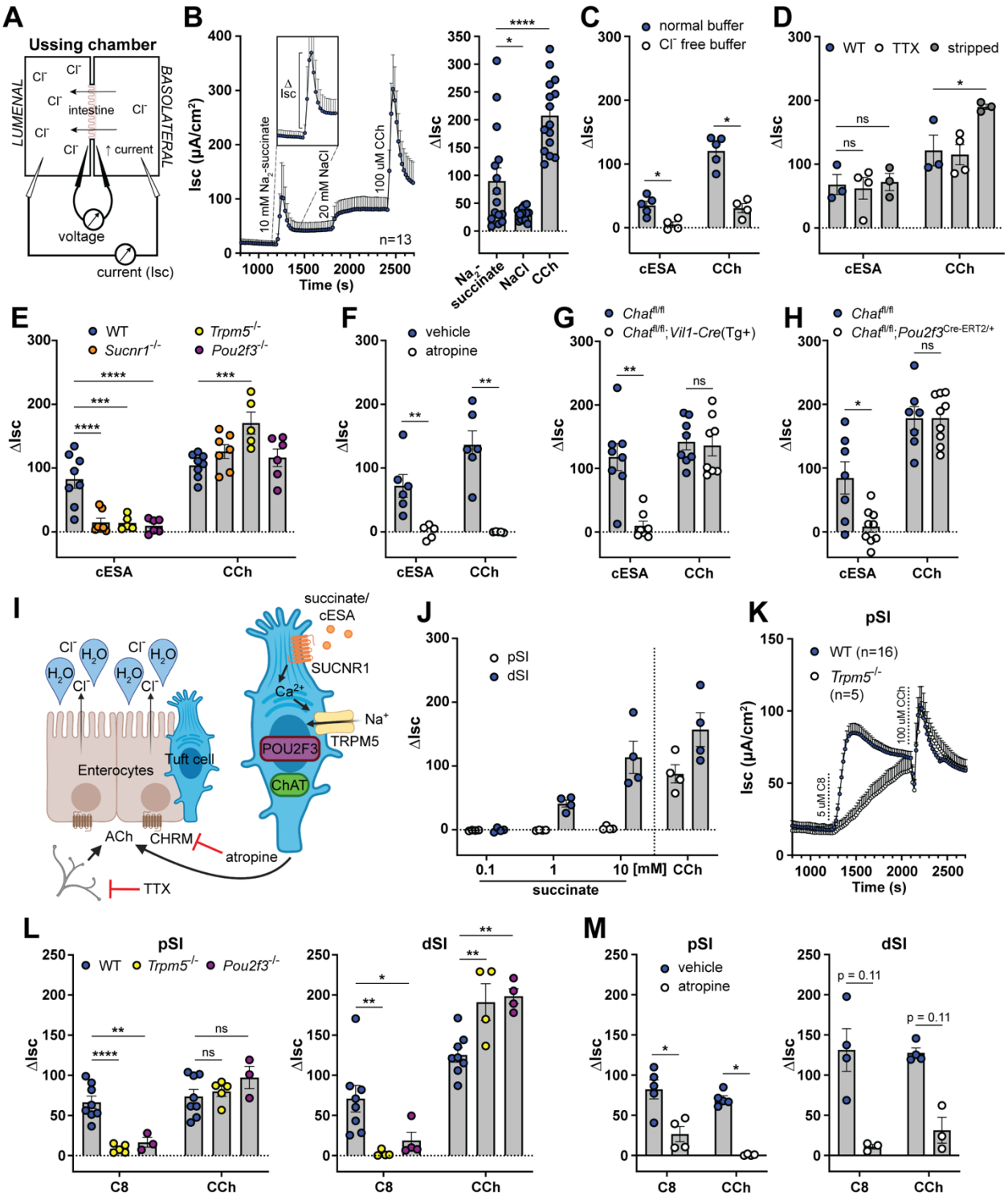

Figure 2: Tuft cell-derived ACh induces epithelial fluid secretion. (**A**) Ussing chamber schematic. (**B**) Average Isc traces and quantification of the delta Isc (ΔIsc, see inset and bar graph) of WT dSI tissue stimulated as indicated (10 mM Na_2-succinate and 20 mM NaCl, lumenal; 100 µM CCh, basolateral). (**C**)

254 ΔIsc values of WT dSI in presence of normal chloride- (Cl^-) containing buffer or buffer selectively lacking
255 Cl^-, stimulated as indicated (10 mM cESA, lumenal). (**D**) ΔIsc values of WT intact dSI compared to
256 stripped dSI and dSI pretreated 15 min with TTX (1 μM, basolateral), stimulated as indicated. (**E**) ΔIsc
257 values of dSI from mice of indicated genotypes stimulated as indicated. (**F**) ΔIsc values of WT dSI
258 compared to dSI pretreated 15 min with pan-CHRM inhibitor atropine (10 μM, basolateral), stimulated as
259 indicated. (**G** and **H**) ΔIsc values of dSI with (G) epithelial cell- (*Vil1-Cre*) and (H) tuft cell-specific
260 (*Pou2f3*$^{ERT2\text{-}Cre/+}$) *Chat* deletion, stimulated as indicated. (**I**) Model of tuft cell chemosensing of succinate
261 driving ACh-dependent fluid secretion independent of neurons. (**J**) ΔIsc values of WT pSI and dSI
262 stimulated as indicated. (**K**) Average Isc traces of pSI from WT or *Trpm5*$^{-/-}$ mice stimulated as indicated (5
263 μM C8, basolateral). (**L** and **M**) ΔIsc values of WT tissues compared to (L) tissues from indicated
264 genotypes or (M) tissues pretreated 15 min with atropine (10 μM, basolateral), stimulated as indicated. In
265 the graphs, each symbol represents an individual mouse (one tissue or average of two) pooled from two
266 or more experiments. Groups represent sequential stimulations of the same tissue. *$p < 0.05$, **$p < 0.01$,
267 ***$p < 0.001$, ****$p < 0.001$ by RM one way ANOVA with Tukey's multiple comparisons test (B), two way
268 ANOVA with Dunnett's multiple comparisons test (D, E, L), multiple Mann-Whitney tests with Holm
269 Sídák's multiple comparisons test (C, F, G, H, M). ns, not significant. Graphs depict mean +/- SEM. Also
270 see Figure S2.
271
272 Since enteric neurons are both a major source of ACh and major regulators of
273 fluid secretion in the intestine, we investigated the possibility that SI tuft cells activate
274 enteric neurons. Studies of *Chat*+ tuft cells in the airways have emphasized their close
275 contact with neurons and provided evidence that signaling can occur from tuft cells to
276 neurons, often via release of ACh.[15,16] We therefore looked for similar tuft-neuronal
277 connections by microscopy using the *Chat-GFP* reporter, which marks cholinergic
278 intestinal neurons as well as tuft cells. We found some instances where a GFP+ tuft cell
279 was approached by a GFP+ neuron, but we never saw neurons extend into the
280 epithelium and contact tuft cells, as they do in the airways (Fig. S2D). *Chat*+ neurons
281 represent only a subset of total intestinal neurons,[55] yet staining for the pan-neuronal
282 marker BIII tubulin (TUJ1) revealed no additional neuronal contacts (Fig. S2E),
283 suggesting that neuronal contacts with tuft cells, much less "synapses", are uncommon
284 in the SI.
285 Recognizing that signaling can occur without direct contact, we experimentally
286 tested the requirement for neurons in the succinate response. First, we disrupted
287 neuronal integrity by physically "stripping" the submucosa off the back of the epithelium

288 to eliminate most of the submucosal and all of the myenteric neuronal plexuses.[51]
289 Alternatively, we used tetrodotoxin (TTX) to inhibit neuronal action potentials in intact SI
290 tissue.[4] Neither treatment reduced the cESA or CCh responses; in the stripped tissue
291 the CCh response was instead increased, likely due to enhanced diffusion (Fig. 2D).
292 Altogether, our data show that succinate/cESA binds to SUCNR1 expressed apically on
293 epithelial cells and induces chloride-dependent fluid secretion, independently of enteric
294 neurons or submucosal tissue.
295 To confirm that tuft cells were the cells that sensed succinate/cESA to initiate the
296 secretion response, we stimulated dSI from tuft cell-deficient *Pou2f3*$^{-/-}$, and
297 chemosensing-deficient *Trpm5*$^{-/-}$ mice. As with SI tissue from *Sucnr1*$^{-/-}$ mice, tissues
298 from these mice failed to respond to cESA (Fig. 2E). Importantly, the CCh response was
299 intact in all knockout mice, demonstrating that the tissue's capacity for ACh-dependent
300 fluid secretion was unaltered. To test whether ACh was involved in the cESA response,
301 we pretreated the dSI with the pan-mAChR inhibitor atropine and found that this
302 completely blocked the cESA and CCh responses (Fig. 2F). Deletion of *Chat* from IECs
303 using *Chat*$^{fl/fl}$*;Vil1-Cre(Tg+)* mice also abrogated the cESA response (Fig. 2G). Although
304 tuft cells are the only *Chat*-expressing IECs, we also deleted *Chat* in tuft cells
305 specifically using *Chat*$^{fl/fl}$*;Pou2f3*$^{Cre\text{-}ERT2/+}$ mice, and confirmed that tuft cell-derived ACh
306 production was required for cESA-induced fluid secretion (Fig. 2H).
307 Other tuft cell effectors (e.g. LTC_4 or PGD_2) have been implicated in acute responses
308 and tuft cells themselves express the receptor for IL-25,[11,56,57] but we excluded the
309 involvement of IL-25 and LTC_4 in ion flux using dSI from *Il25*$^{-/-}$ and *Alox5*$^{fl/fl}$*;Vil1-*
310 *Cre1000(Tg+)* mice, respectively (Fig. S2F,G). Pretreatment with the COX inhibitor
311 ibuprofen to block PGD_2 synthesis also did not affect the cESA response (Fig. S2H).
312 Furthermore, PGD_2, which has not been previously linked with fluid secretion but has
313 been reported to induce mucus secretion from goblet cells (GCs) in the colon,[56] did not
314 induce ion flux in the dSI (or the colon) when administered basolaterally (Fig. S2I). We
315 also investigated the possibility that tuft cells were signaling to neighboring cells via gap
316 junctions.[58] The gap junction inhibitor carbenoxolone partially blocked cAMP-driven fluid
317 secretion induced by IBMX + forskolin, but had no effect on cESA or CCh responses
318 (Fig. S2J). Thus, we have demonstrated that tuft cells in the dSI sense lumenal

succinate/cESA and release ACh basolaterally, which stimulates mAChR-dependent Cl^- ion secretion (Fig. 2I). The response is epithelium-intrinsic and does not involve enteric neurons.

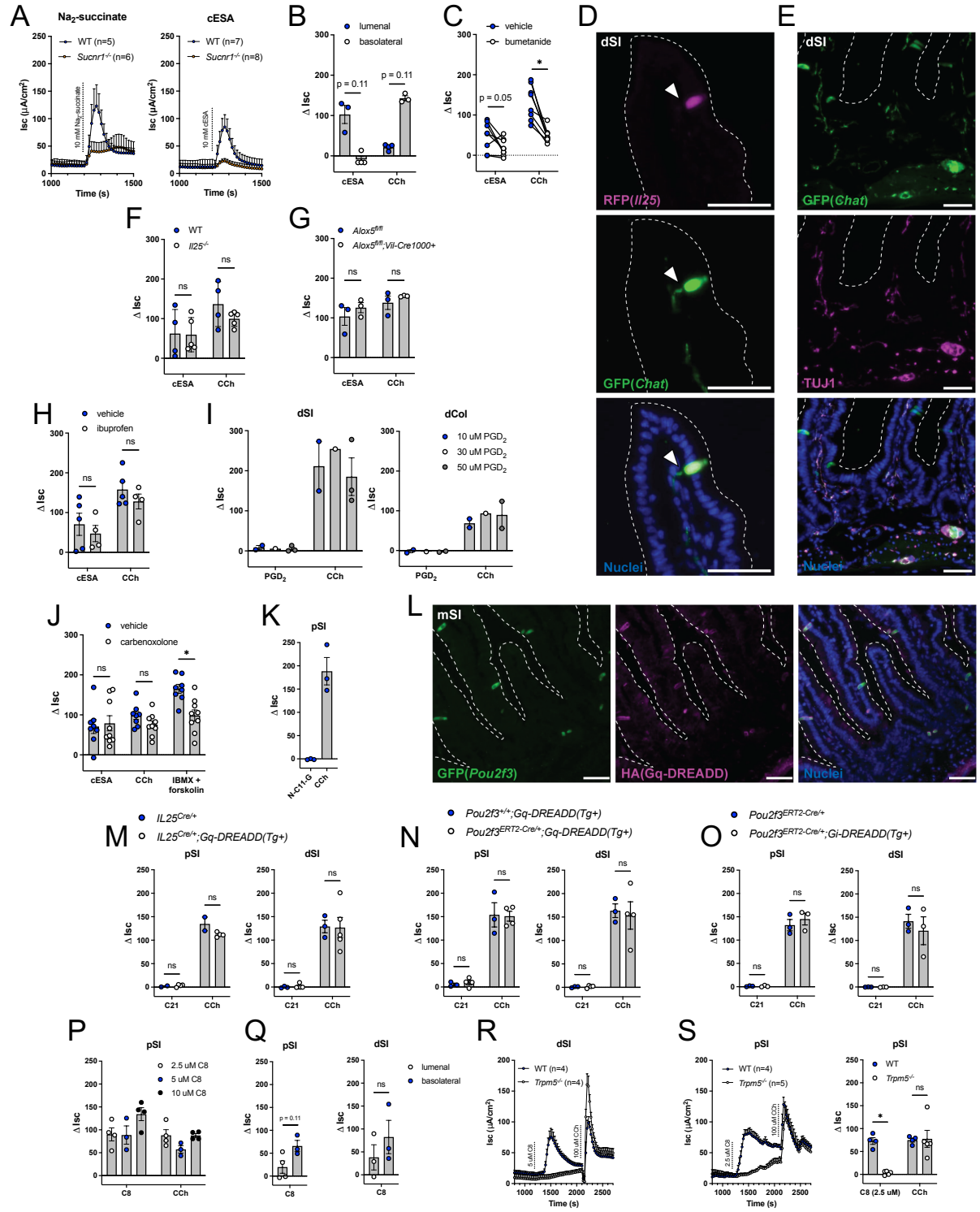

323 **Supplemental Figure 2:** (**A**) Average Isc traces of dSI from WT or *Sucnr1*$^{-/-}$ mice stimulated as indicate
324 (Na_2-succinate and cESA, lumenal). (**B**) ΔIsc values of WT dSI stimulated as indicated. (**C**) ΔIsc values of
325 WT dSI pretreated 15 min with vehicle or bumetanide (100 μM, basolateral), stimulated as indicated (10
326 mM cESA lumenal; 100 μM CCh, basolateral). (**D**) Representative immunofluorescence image of a GFP+
327 (green) neuronal process (indicated by solid white arrow) approaching a GFP+/RFP+ (magenta) tuft cell
328 from the dSI of *Chat-GFP*;*Il25*$^{RFP/+}$ mice. Nuclei stained with DAPI (blue). Scale bars: 50 μm. (**E**)
329 Representative immunofluorescence image of GFP+ (green) neurons co-stained for BIII tubulin (TUJ1,
330 magenta) in the dSI. Nuclei stained with DAPI (blue). Scale bars: 50 μm. (**F**, **G**, and **H**) (F and G) ΔIsc
331 values of dSI from indicated genotypes or (H) WT dSI compared to dSI pretreated 15 min with ibuprofen
332 (10 μM, bilateral), stimulated as indicated. (**I**) ΔIsc values of WT tissues stimulated as indicated (PGD_2,
333 basolateral). (**J**) ΔIsc values for WT dSI compared to dSI pretreated 15 min with carbenoxolone (1 mM,
334 lumenal), stimulated as indicated (100 μM IBMX + 10 μM forskolin, bilateral). (**K**) ΔIsc values of WT pSI
335 stimulated as indicated (100 μM N-C11-G, lumenal). (**L**) Representative immunofluorescence image of
336 GFP+ (green) tuft cells expressing HA+ Gq-DREADDs (magenta) in the crypts and villi of the medial SI
337 (mSI). Nuclei stained with DAPI (blue). Scale bars: 50 μm. (**M**, **N**, and **O**) (M) ΔIsc values of indicated
338 tissues from unmanipulated mice or (N and O) indicated tissues from mice 7 days after start of tamoxifen
339 chow, stimulated as indicated (1 μM C21, bilateral). (**P**) ΔIsc values of WT pSI stimulated as indicated
340 (C8, bilateral). (**Q**) ΔIsc values of WT tissues from pSI and dSI stimulated as indicated. (**R**) Average Isc
341 traces of dSI stimulated as indicated (5 μM C8, basolateral). (**S**) Average Isc traces and ΔIsc values of
342 pSI stimulated as indicated (2.5 μM C8, basolateral). In the graphs, each symbol represents an individual
343 mouse (one tissue or average of two) pooled from two or more experiments. Groups represent sequential
344 stimulations of the same tissue. In (C) paired vehicle and bumetanide-treated tissues are from the same
345 mouse. *$p < 0.05$, **$p < 0.01$, ***$p < 0.001$, ****$p < 0.001$ by multiple Mann-Whitney tests with Holm
346 Sídák's multiple comparisons test (B, F-H, J, M-O, S), Wilcoxon matched-pairs signed rank test with Holm
347 Sídák's multiple comparisons test (C), or Mann-Whitney test (Q). ns, not significant. Graphs depict mean
348 +/- SEM.
349

350 ***A TRPM5 agonist induces tuft- and ACh-dependent fluid secretion in the pSI and***
351 ***dSI***

352 In characterizing the succinate response, we found that the pSI did not respond
353 to succinate stimulation (Fig. 2J). This finding is consistent with greater succinate
354 receptor (*Sucnr1*) expression in tuft cells from the dSI compared to the pSI (Table S2),[23]
355 and may also reflect the reduced frequency of *Chat*+ tuft cells in the pSI (Fig. 1D). Since
356 the pSI was responsive to CCh, we reasoned that pSI tuft cells could induce fluid
357 secretion if properly stimulated. We first tested several putative tuft cell ligands. Worm

358 excretory and secretory products from *Nippostrongylus brasiliensis* (*Nb*), known as
359 NES, failed to stimulate ion flux whether made from infective L3 larvae or adult worms
360 (data not shown). The bacterial metabolite N-C11-G did not induce ion flux either (Fig.
361 S2K). Next, we tried a chemogenetic approach with Gq- or Gi-coupled receptors that
362 respond only to synthetic ligands (DREADDs)[59] using constitutive (*Il25-Cre*) or inducible
363 (*Pou2f3*$^{Cre\text{-}ERT2/+}$) for tuft cell-specific expression. Although tuft cells expressed the HA
364 tag included in the DREADD constructs, stimulation with Compound 21[60] was
365 insufficient to drive a fluid secretion response in the pSI or dSI (Fig. S2L-O). Perhaps G
366 proteins required for DREADD function are not available in tuft cells or the signals
367 induced downstream of DREADD activation are not sufficient to induce ACh release.
368 Finally, we decided to stimulate TRPM5 directly, since all tuft cell chemosensing
369 pathways identified to date converge on TRPM5. We acquired a TRPM5 agonist
370 compound called Class 8 (C8),[61,62] and found that it induced ion flux in both the pSI and
371 dSI when administered lumenally or basolaterally, with a trend toward higher basolateral
372 responses (Fig. 2K, S2P-Q). The C8 response was similar to cESA- or CCh-induced ion
373 flux, and was TRPM5-dependent in the pSI and dSI (Fig. 2K-L, S2R). The C8 response
374 was also tuft cell- and ACh-dependent in both locations (Fig. 2L-M). In the pSI, C8
375 induced a slow TRPM5-independent increase in Isc (Fig. 2K), but this off-target effect
376 could be eliminated by lowering the dose of C8 (Fig. S2S). We conclude that in
377 response to direct TRPM5 activation, tuft cells in the pSI and dSI can release ACh to
378 induce fluid secretion from the intestinal epithelium.
379
380 ***Tuft cell-mediated fluid secretion occurs across mucosal tissues and is***
381 ***detectable in vivo***
382 We previously found that *Sucnr1* expression is even higher in tracheal tuft cells
383 than those of the SI,[11] so to test if tuft cells regulate fluid secretion at multiple mucosal
384 barriers, we stimulated tracheal tissue in the Ussing chamber with succinate. As in the
385 dSI, we found that this induced a rapid increase in the Isc that was *Pou2f3*-, *Sucnr1*-,
386 and *Trpm5*-dependent (Fig. 3A-B). In addition, the response was mAChR-dependent
387 (Fig. 3C). By comparison, the cecum and colon, where tuft cells express *Sucnr1* at low
388 levels,[11] responded only weakly to succinate stimulation and in a tuft-independent

389 manner (Fig. S3A). Colonic tissue did respond to TRPM5 agonism with C8, with a larger
390 response in the proximal colon (pCol) than the distal colon (dCol) (Fig. 3D-E). The
391 reported tuft ligand N-C11-G[56] did not stimulate fluid secretion from the dSI or dCol (Fig.
392 S3B), and also failed to elicit tuft-dependent leukotriene production from intestinal
393 epithelial monolayers (Fig. S3C). Therefore, tuft cell control of epithelial fluid secretion is
394 a common effector function across barrier tissues.
395 The Ussing chamber measures ion flux but cannot measure water movement
396 directly. We therefore wanted to test if activating tuft cells *in vivo* could induce fluid
397 secretion into the intestine. We dosed mice with C8 or vehicle in the morning and then
398 measured the wet weight of fecal pellets 3 hours later. In mice given vehicle, the fecal
399 water content declined, likely due to reduced water intake during the day. C8 treatment
400 prevented this decline, indicating sustained fluid secretion (Fig. 3F). Importantly, this
401 fluid secretion was dependent on epithelial *Chat* (Fig. 3G, S3D). Thus, activation of tuft
402 cells along the intestinal tract induces ACh-dependent ion flux that drives fluid secretion
403 into the intestinal lumen.

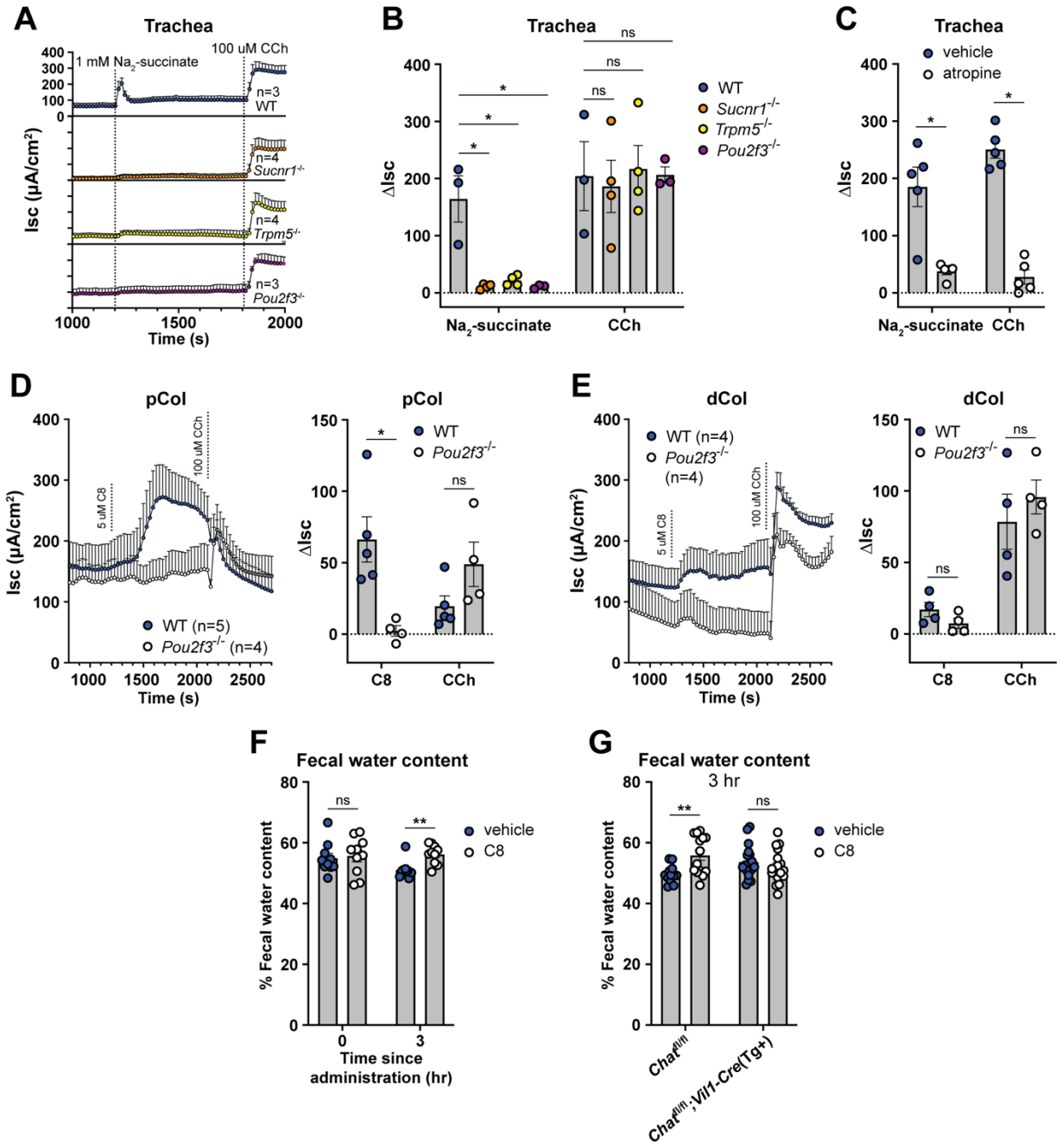

Figure 3: ***Tuft cell-mediated fluid secretion occurs across mucosal tissues and is detectable in vivo.*** (**A** and **B**) (A) Average Isc traces and (B) ΔIsc values of trachea from mice of indicated genotypes stimulated as indicated (1 mM Na_2-succinate, lumenal; 100 μM CCh, basolateral). (**C**) ΔIsc values of WT trachea compared to trachea pretreated 15 min with atropine (10 μM, basolateral), stimulated as indicated. (**D** and **E**) Average Isc traces and ΔIsc values of WT and *Pou2f3*$^{-/-}$ tissues stimulated as indicated (5 μM C8, basolateral). (**F** and **G**) Quantification of water content of fecal pellets collected from (A) WT or (B) *Chat-fl;Vil1-Cre(Tg+)* mice treated orally with vehicle or C8 (30 mg/kg) for the indicated durations. In the graphs, each symbol represents an individual mouse (one tissue or average of two)

413 pooled from two or more experiments. Groups represent sequential stimulations or timepoints of the same
414 tissue or animal. *p < 0.05, **p < 0.01, ***p < 0.001, ****p < 0.001 by, two way ANOVA with Tukey's
415 multiple comparisons test (B), or multiple Mann-Whitney tests with Holm Sídák's multiple comparisons
416 test (C-G). ns, not significant. Graphs depict mean +/- SEM. Also see Figure S3.
417

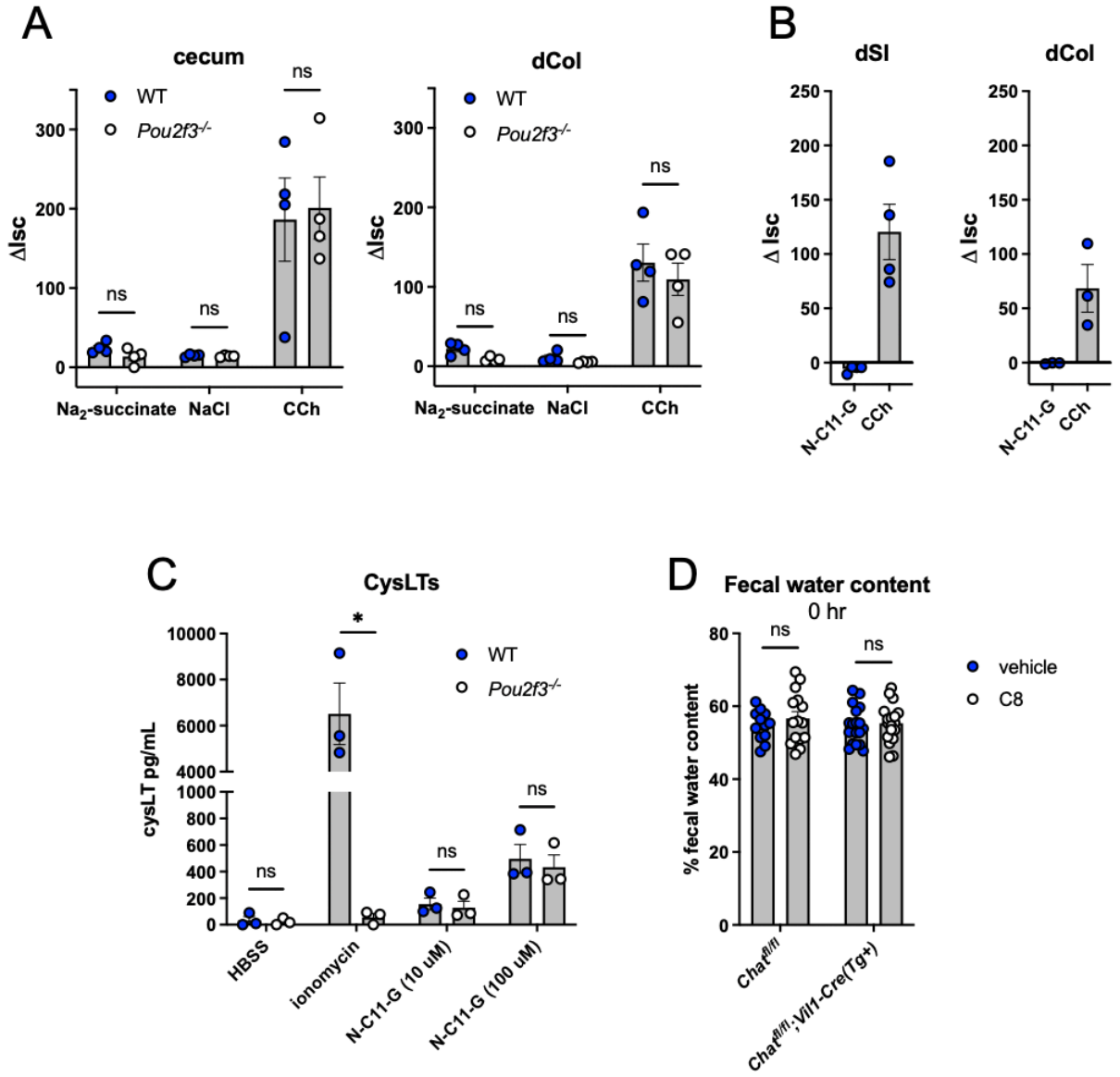

418

419 **Supplemental Figure 3:** (**A**) ΔIsc values of WT and *Pou2f3*$^{-/-}$ tissues stimulated as indicated (10 mM Na_2-
420 succinate and 20 mM NaCl, lumenal; 100 μM CCh, basolateral). (**B**) ΔIsc values of WT tissues stimulated
421 as indicated (100 μM N-C11-G, lumenal). (**C**) Cysteinyl leukotriene (CysLTs) production from WT and
422 *Pou2f3*$^{-/-}$ SI epithelial monolayers stimulated as indicated. (**D**) Quantification of water content of fecal
423 pellets collected from indicated mice immediately after oral treatment with C8 (30 mg/kg). In the graphs,
424 each symbol represents an individual mouse pooled from two or more experiments. In (A-B) groups

425 represent sequential stimulations of the same tissue and in (C) groups represent individual monolayers.
426 *p < 0.05, **p < 0.01, ***p < 0.001, ****p < 0.001 by multiple Mann-Whitney tests with Holm Sídák's
427 multiple comparisons test (A, D), or multiple unpaired t tests with Holm Sídák's multiple comparisons test
428 (C). ns, not significant. Graphs depict mean +/- SEM.
429

430 ***Tuft cell-derived ACh is not required for ILC2 activation***

431 Having defined ACh-dependent fluid secretion as a tuft cell effector function in
432 unmanipulated mice, we next considered the role of tuft cell-derived ACh during Type 2
433 immunity. Consistent with previous reports in the airways,[63] we found that tamoxifen
434 partially suppressed Type 2 responses in the intestine. For example, treating protist-
435 colonized *Chat*$^{fl/fl}$*;Pou2f3*$^{Cre\text{-}Ert2/+}$ mice with tamoxifen for one week reduced tuft cell
436 counts by nearly half in both WT and Cre+ mice (Fig. S4A). The effect of tamoxifen was
437 less noticeable during helminth infection, perhaps because this induces more Type 2
438 inflammation (Fig. S4B). Nonetheless, given these non-specific effects of tamoxifen, we
439 focused on identifying *Chat*-dependent effects by analyzing *Chat*-sufficient and *Chat*-
440 deficient mice that had all been treated with tamoxifen.

441 Previously characterized SI tuft cell effector molecules (e.g. IL-25 and LTC_4)
442 have primarily been shown to regulate ILC2 activation.[21,27] Also, recent studies have
443 reported that ILC2s express *Chat* following activation and that ACh can potentiate their
444 production of cytokines and proliferation, perhaps via autocrine signaling[64,65]. We
445 therefore asked if tuft cell-derived ACh was signaling to ILC2s in addition to inducing
446 fluid secretion. We began by testing if ACh could enhance ILC2 activation using an *in*
447 *vitro* model of acute (6-hour) ILC2 stimulation.[27] Pairing ACh with IL-25 to mimic the
448 results of tuft cell activation, we failed to detect any ACh-dependent ILC2 activation as
449 measured by IL-13 reporter expression and secretion of IL-13 and IL-5 (Fig. S4C-D). By
450 contrast, LTC_4 greatly enhanced ILC2 activation when given with IL-25, as expected.
451 We conclude that ACh does not induce cytokine expression in ILC2s sorted from
452 unmanipulated mice and is therefore unlikely to contribute to their initial activation.
453

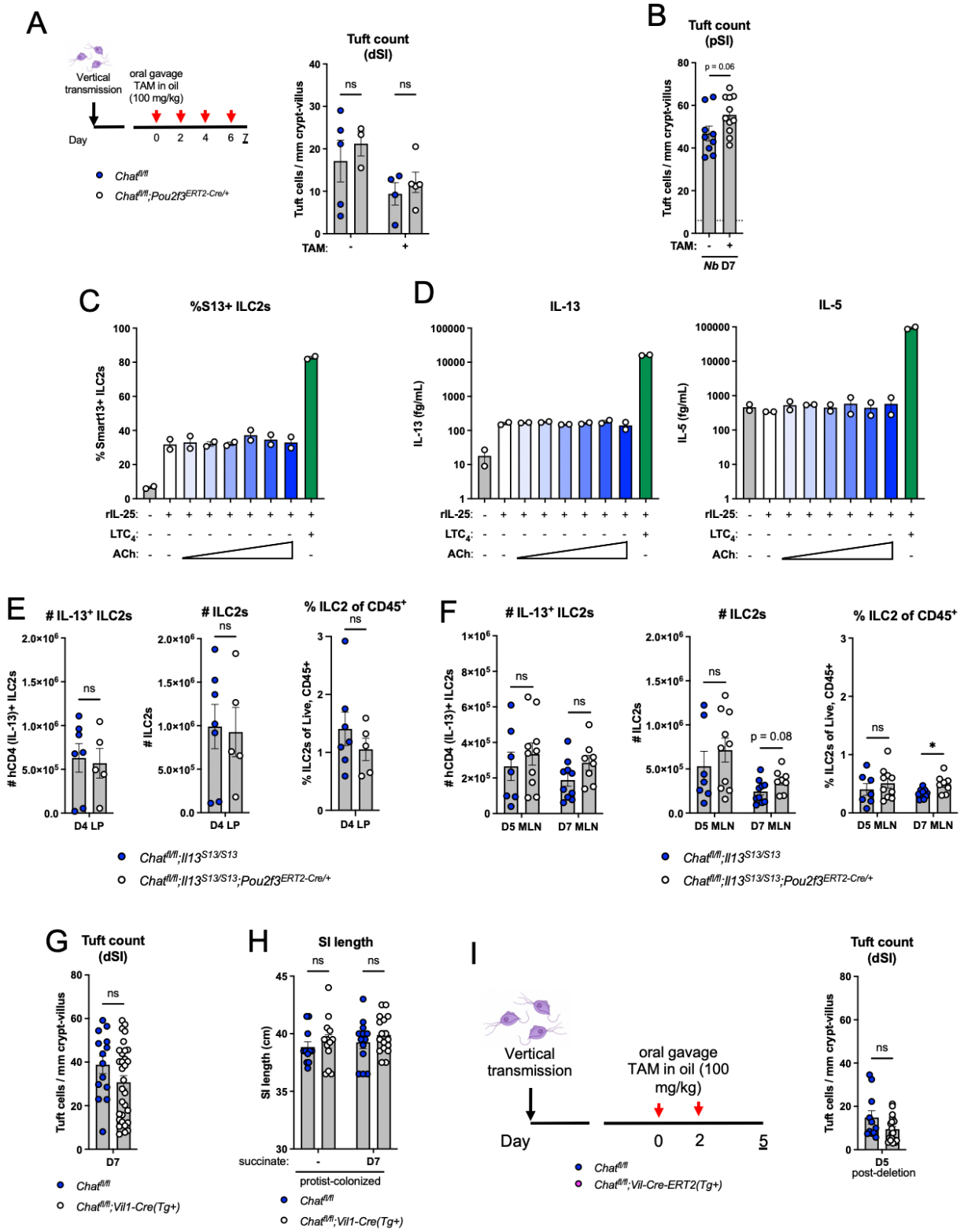

Supplemental Figure 4: (**A**) Schematic of tamoxifen (TAM) treatment of protist-colonized *Chat-fl; Pou2f3*$^{ERT2\text{-}Cre/+}$ mice and quantification of dSI tuft counts by immunofluorescence at D7 after start of treatment. (**B**) Quantification of pSI tuft counts by immunofluorescence of WT mice treated with or without

458 tamoxifen and infected with *Nb* for 7 days. (**C** and **D**) (C) Flow cytometric quantification of percent hCD4+
459 (IL-13+) SILP ILC2s and (D) IL-13 and IL-5 concentration in their supernatant after 6 hr *in vitro* culture
460 with the indicated conditions (0.1 ng/mL rIL-25, serial 10-fold dilutions of ACh from 10 mM to 0.1 μM, 1
461 nM LTC_4). (**E** and **F**) Quantification of number of hCD4+ (IL-13+) ILC2s, total ILC2s, and percent ILC2s at
462 the indicated timepoints, tissues, and genotypes. (**G**) Quantification of dSI tuft counts by
463 immunofluorescence from indicated mice treated with 150 mM succinate drinking water for 7 days. (**H**) SI
464 length from indicated mice vertically-colonized with *T. rainier* protists with or without 7 days of additional
465 150 mM succinate drinking water treatment. (**I**) Schematic of acute deletion of *Chat* from vertically *T.*
466 *musculis* (*Tm*) -colonized mice and quantification of dSI tuft counts by immunofluorescence 5 days after
467 start of treatment. In the (A-B, E-I), each symbol represents an individual mouse from two or more pooled
468 experiments. In (C and D) each symbol represents a technical replicate of cells sorted from pooled mice.
469 *p < 0.05, **p < 0.01, ***p < 0.001, ****p < 0.001 by multiple Mann-Whitney tests with Holm Sídák's
470 multiple comparisons test (A, F, H) or Mann-Whitney test (B, E, G, I). ns, not significant. Graphs depict
471 mean +/- SEM.
472
473 To test if tuft cell-derived ACh was involved in ILC2 activation *in vivo* and at later
474 timepoints, we generated *Chat*$^{fl/fl}$*;Pou2f3*$^{ERT2\text{-}Cre/+}$ mice that also expressed an IL-13
475 reporter (Smart13). We treated these mice with tamoxifen, infected with *Nb*, and
476 assessed early ILC2 activation in the LP 4 days post infection (dpi), about 2 days after
477 the worms arrive in the intestine. We found no difference in ILC2 activation or expansion
478 (Fig. 4A, S4E). Since *Chat* has been detected in activated but not resting ILC2s, we
479 also tested if tuft cell-derived ACh regulated ILC2s later during infection. Given the
480 difficulty of isolating viable cells from Type 2 inflamed SI, we assessed ILC2s in the
481 mesenteric lymph nodes at 5 and 7 dpi. Again, we saw equivalent activation and
482 expansion of ILC2s between *Chat*-sufficient and -deficient mice (Fig. 4B, S4F). We
483 conclude that tuft cell-derived ACh does not contribute to ILC2 activation during
484 helminth infection of the SI.
485
486 ***Tuft cell-derived ACh is not required for Type 2 intestinal remodeling***
487 An effective immune response to helminths requires intestinal remodeling, such
488 as hyperplasia of tuft cells and mucus-producing GCs and lengthening of the SI.[23,66] IL-
489 13 is critical for this process, but ACh might also contribute. For example, ACh has been

490 implicated in direct modulation of epithelial cell differentiation,[67,68] and could also impact
491 tissue remodeling via other AChR-expressing cells, such as neurons.[55]
492 Using tuft cell frequency, goblet cell frequency, and intestinal length as markers
493 of SI remodeling, we found little or no defect 7 days after *Nb* infection of mice with either
494 constitutive (*Vil1-Cre(Tg+)*) or acute (*Vil1-Cre-Ert2(Tg+)*) deletion of *Chat* in IECs (Fig.
495 4C-E). The same was true both 5 and 7 days after *Nb* infection when we used *Pou2f3-*
496 *Cre-ERT2* for tuft cell-specific *Chat* deletion (Fig. 4F-H). Since tuft cell circuits are
497 distinct in the pSI and dSI,[11,27] we also tested Type 2 remodeling in the dSI 4 and 7
498 days after starting treatment with succinate-supplemented drinking water. As before,
499 there was little effect of either constitutive or inducible IEC *Chat* deletion (Fig. 4I-K;
500 S4G). Likewise, *Chat*$^{fl/fl}$*;Vil1-Cre(Tg+)* mice vertically colonized with protists had no
501 defect in tuft cell hyperplasia or SI length at homeostasis or following one week of
502 additional succinate drinking water treatment (Fig. 4L, S4H). Acute loss of *Chat* in
503 protist-colonized *Chat*$^{fl/fl}$*;Vil1-Cre-ERT2(Tg+)* mice also had no effect on tuft cell
504 hyperplasia 5 days later (Fig. S4I). In sum, Type 2 remodeling is broadly intact in the
505 absence of tuft cell ACh. We did observe small but significant decreases in tuft cell
506 hyperplasia or SI lengthening in some assays, but this effect was inconsistent and
507 minimal compared to loss of other tuft cell effector molecules (e.g. IL-25 and LTC_4).[21,27]
508
509

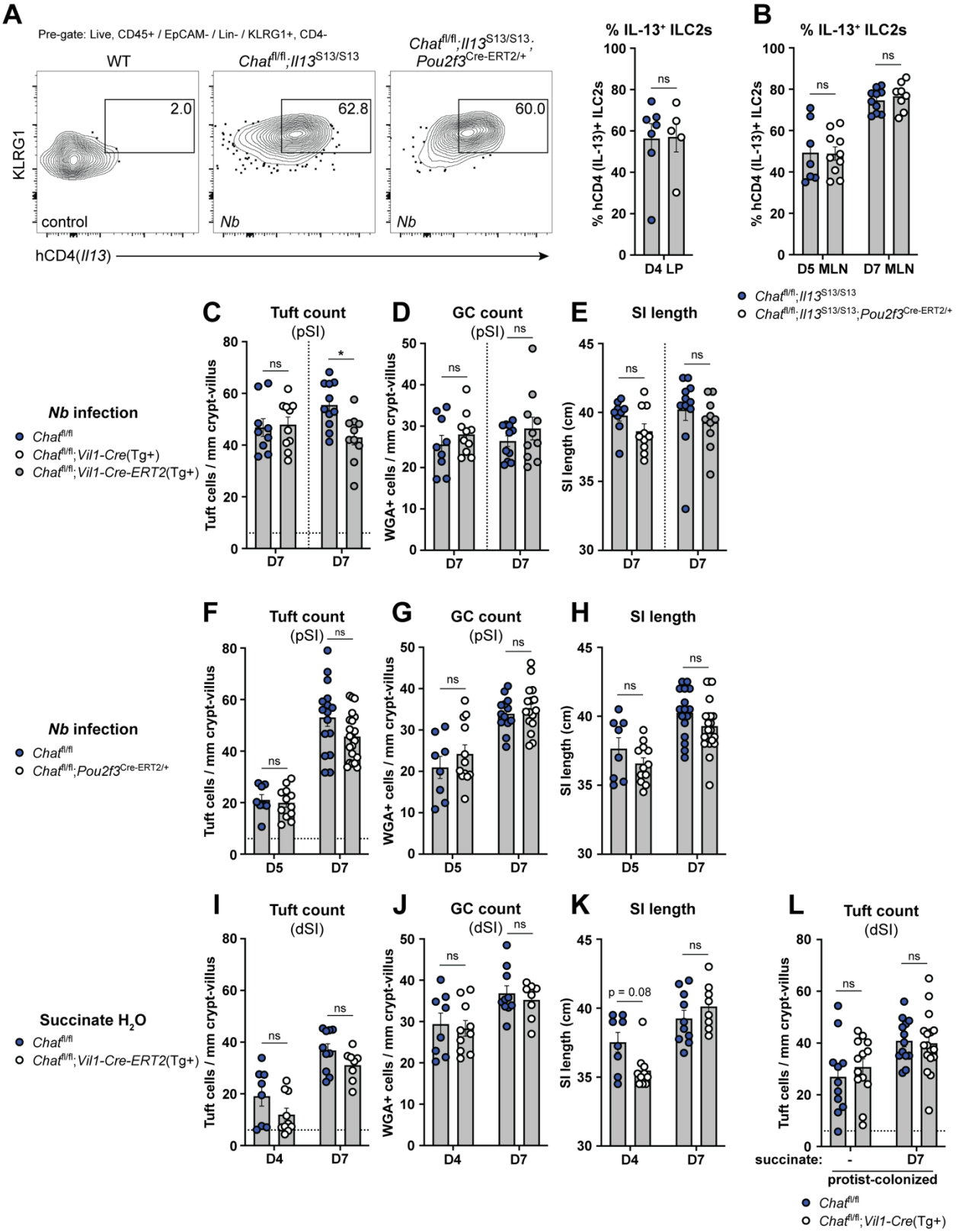

510

511 **Figure 4: Tuft cell-derived ACh is not required for ILC2 activation or intestinal remodeling.** (**A** and

512 **B**) (A) Representative flow cytometry and quantification of percent hCD4^{+} (IL-13^{+}) ILC2s (Lin^{-}, CD45^{+},

513 KLRG1^{+}, CD4^{-}) in the SI LP and (B) mesenteric lymph nodes (MLN) at the indicated *Nb* infection
514 timepoints. (**C**, **D**, and **E**) (C) Quantification of pSI tuft cells (DCLK1+) and (D) goblet cells (WGA+) by
515 immunofluorescence and (E) total SI length from the indicated mice at D7 of *Nb* infection. (**F**, **G**, and **H**)
516 Same analysis as in C-E in the indicated mice at the indicated *Nb* infection timepoints. (**I**, **J**, and **K**) Same
517 analysis as in C-E in the indicated mice at the indicated timepoints of 150 mM succinate drinking water
518 treatment. (**L**) Quantification of tuft cells (DCLK1+) by immunofluorescence from indicated mice vertically-
519 colonized with *T. rainier* protists with or without 7 days of additional 150 mM succinate drinking water
520 treatment. In the graphs, each symbol represents an individual mouse from two or more pooled
521 experiments. For graphs of tuft cell counts, horizontal dashed line signifies baseline tuft cell count in
522 unmanipulated mice. *$p < 0.05$, **$p < 0.01$, ***$p < 0.001$, ****$p < 0.001$ by Mann Whitney test (A) or
523 multiple Mann-Whitney tests with Holm Sídák's multiple comparisons test (B-L). ns, not significant.
524 Graphs depict mean +/- SEM. Also see Fig. S4.
525

526 ***Tuft cell hyperplasia results in enhanced ACh-dependent fluid secretion***

527 The ability of tuft cells to induce fluid secretion in the steady state led us to ask
528 how it would change during Type 2 inflammation, when tuft cell numbers can increase
529 10-fold and fluid secretion might support worm clearance as part of the canonical weep
530 and sweep response. First, we asked whether the number and frequency of *Chat*+ tuft
531 cells changed with Type 2 inflammation. While the frequency of *Chat*+ tuft cells
532 decreased (Fig. S5A), this was more than compensated for by the hyperplasia, such
533 that the total number of *Chat*+ tuft cells per millimeter crypt/villus was increased in the
534 pSI and especially the dSI 7 days after either succinate-treatment or *Nb*-infection (Fig.
535 5A).

536 Next, we infected mice with *Nb* to induce tuft cell hyperplasia and quantified the
537 fluid secretion response to succinate in the pSI and dSI across the course of infection.
538 Although pSI tuft cells do not respond to succinate at steady state, we wondered if
539 those that emerge during infection might be responsive. The pSI did not become
540 responsive to succinate (or cESA) over the course of infection, but the dSI succinate
541 response increased by day 7, when tuft cell numbers peaked (Fig. 5B, S5B-C). The
542 increased response to succinate was less than the ~3-fold increase of *Chat*+ tuft cells
543 that we observed on D7 of *Nb* infection, likely because the epithelium's total capacity to
544 respond to ACh/CCh was reduced by Type 2 inflammation, as previously reported (Fig.
545 5B).[69]

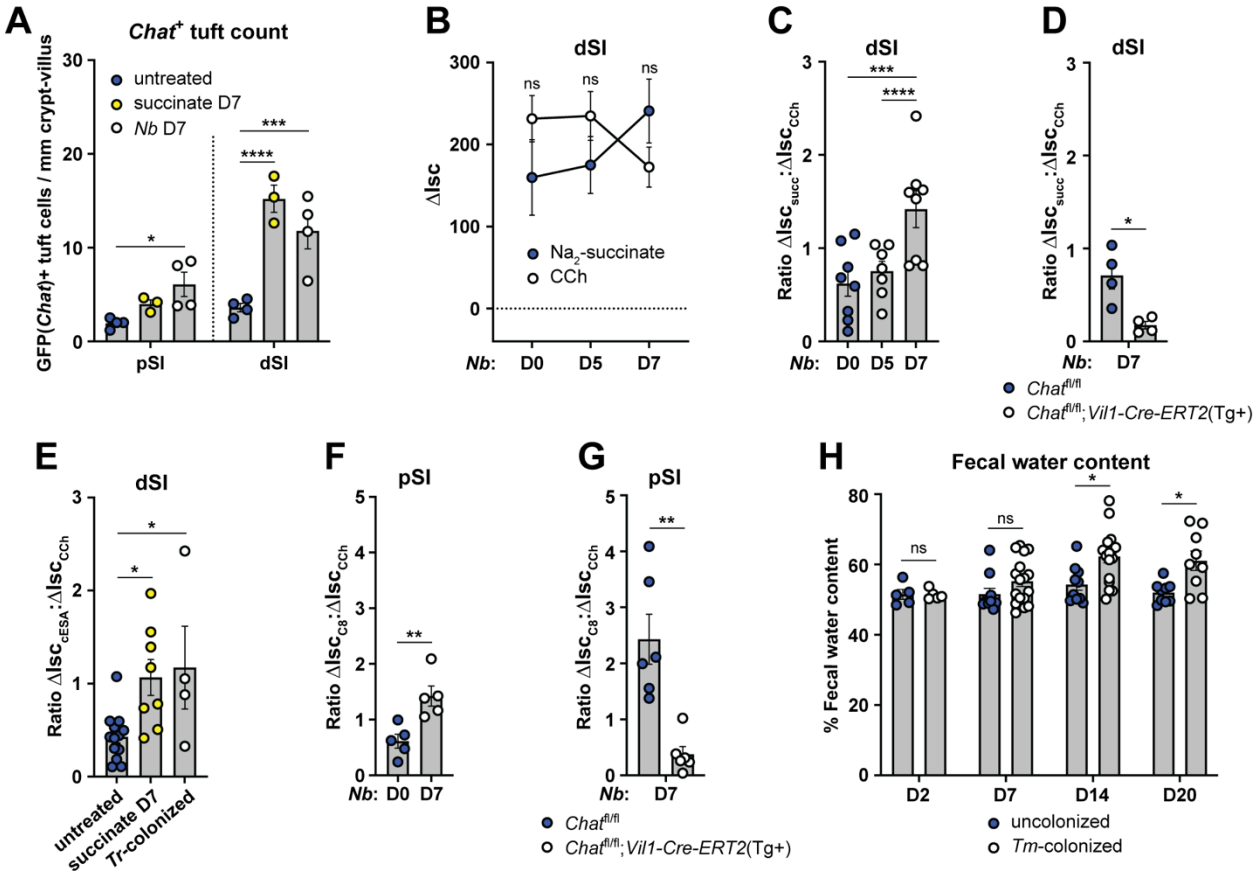

Figure 5: Tuft cell hyperplasia results in enhanced ACh-dependent fluid secretion. (**A**) Quantification of GFP(*Chat*)+ tuft cells (*Il25*-RFP+) from the pSI and dSI of WT mice untreated, treated with 150 mM Na_2-succinate drinking water (succinate), or infected with *N. brasiliensis* (*Nb*) for 7 days. (**B**) ΔIsc values of dSI from WT mice infected with *Nb* for the indicated number of days and stimulated as indicated (10 mM succinate, lumenal; 100 μM CCh, basolateral). (**C**) Ratio of succinate ΔIsc values to CCh ΔIsc values of dSI from (B). (**D**) Ratio of succinate ΔIsc values to CCh ΔIsc values of dSI of indicated mice 7 days after *Nb* infection. (**E**) Ratio of cESA ΔIsc values to CCh ΔIsc values of dSI from WT mice treated with succinate (as in A) or vertically colonized with *T. rainier* (*Tr*) protists. (**F** and **G**) Ratio of C8 ΔIsc values to CCh ΔIsc values of pSI from (F) WT or (G) mice of indicated genotypes mice at indicated timepoints after *Nb* infection. (**H**) Quantification of water content of fecal pellets collected at indicated timepoints post *T. musculis* (*Tm*) colonization of WT mice. In the graphs, each symbol represents an individual mouse pooled from two or more experiments. *p < 0.05, **p < 0.01, ***p < 0.001, ****p < 0.001 by two way ANOVA with Dunnett's multiple comparisons test (A), Mann-Whitney test (B, D, F-G), one way ANOVA (C, E), or multiple Mann-Whitney tests with Holm Sídák's multiple comparisons test (H). ns, not significant. Graphs depict mean +/- SEM. Also see Fig. S5.

563 This effect could be quantified by measuring the ratio of succinate-induced ΔIsc to CCh-
564 induced ΔIsc (Fig. 5C), highlighting how hyperplasia allows tuft cells to capture a greater
565 proportion of the total epithelial ACh response. We confirmed that the increased
566 succinate response on day 7 still required epithelium-derived ACh (Fig. 5D, S5D) and
567 did not occur without *Sucnr1* (Fig. S5E). Enhanced succinate/cESA-induced fluid
568 secretion was also observed if tuft cell hyperplasia was established with oral succinate
569 or *Tritrichomonas* colonization (Fig. 5E). We found that tuft cell hyperplasia induced by
570 *Nb* infection also increased C8-dependent fluid secretion in both the pSI and dSI, and
571 that this required epithelial *Chat* (Fig. 5F-G, S5F-K).
572 To further test the hypothesis that increased numbers of tuft cells drive increased
573 succinate-induced fluid secretion during Type 2 remodeling, we turned to Balb/c mice.
574 Unmanipulated Balb/c mice are nearly tuft cell-deficient in the dSI, but activation of
575 ILC2s with exogenous IL-25 increases tuft cell numbers (Fig. S5L).[44] Accordingly,
576 unmanipulated Balb/c dSI did not respond to cESA in the Ussing chamber, but
577 responsiveness was induced by rIL-25 treatment, indicating that increased numbers of
578 ACh-producing tuft cells were needed (Fig. S5M).
579 Lastly, to test if *in vivo* fluid secretion was enhanced during Type 2 remodeling,
580 we measured the fecal water content of protist-colonized mice. Compared to
581 uncolonized mice, mice colonized with the succinate-producing protist *T. musculis* had
582 increased fecal water content by 14 and 20 days after colonization (Fig. 5H). This
583 suggested that tuft cells were repeatedly responding to protist-derived succinate and
584 inducing fluid secretion. Thus, the increased number of *Chat*+ tuft cells induced during
585 SI Type 2 inflammation drives increased ACh-dependent fluid secretion despite an
586 overall desensitization of the tissue to ACh.

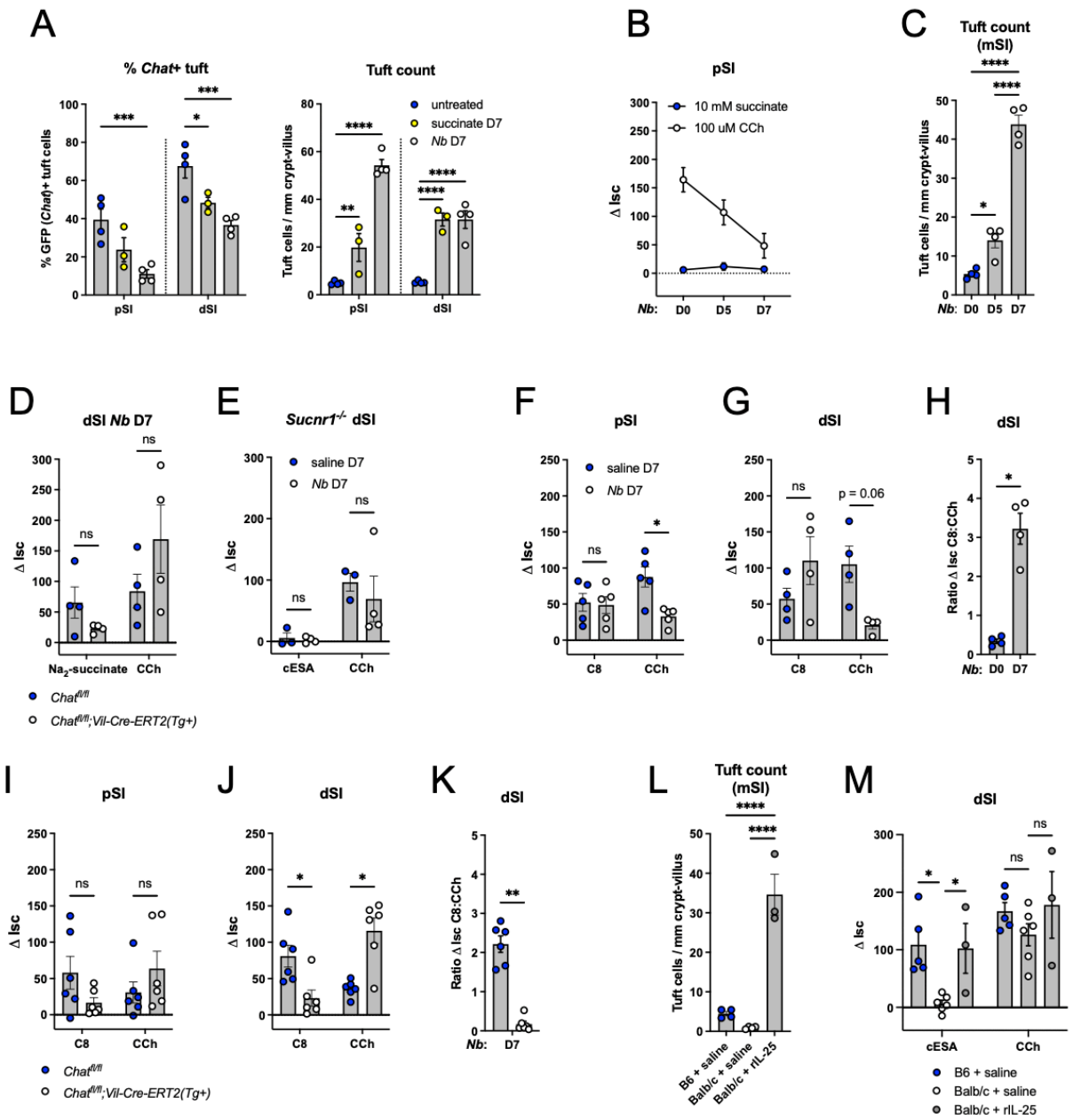

Supplemental Figure 5: (**A**) Quantification of percent GFP(*Chat*)+ tuft cells and RFP(*Il25*)+ tuft cells from the pSI and dSI of WT mice untreated, treated with 150 mM Na_2-succinate drinking water (succinate), or infected with *N. brasiliensis* (*Nb*) for the duration indicated. (**B**) ΔIsc values of pSI from WT mice infected with *Nb* for the indicated number of days and stimulated as indicated (10 mM succinate, lumenal; 100 μM CCh, basolateral). (**C**) Quantification of tuft cells (DCLK1+) by immunofluorescence from medial SI (mSI) of mice in (B). (**D**) ΔIsc values of dSI from mice of indicated genotypes infected with *Nb* for 7 days and stimulated as indicated. (**E**) ΔIsc values of *Sucnr1*$^{-/-}$ dSI with or without 7 day *Nb* infection, stimulated as indicated. (**F-G**) ΔIsc values of (F) pSI and (G) dSI from WT mice with or without 7 day *Nb* infection, stimulated as indicated. (**H**) Ratio of C8 ΔIsc values to CCh ΔIsc values in (G). (**I** and **J**) ΔIsc values of (I)

597 pSI and (J) dSI from mice of indicated genotype infected with *Nb* for 7 days, stimulated as indicated. (**K**)
598 Ratio of C8 ΔIsc values to CCh ΔIsc values from (J). (**L**) Quantification of tuft cells (DCLK1+) by
599 immunofluorescence in the mSI of mice of indicated genotypes treated as indicated. (**M**) ΔIsc values of
600 dSI from mice in (L) stimulated as indicated. In the graphs, each symbol represents an individual mouse
601 (one tissue or average of two) from two or more pooled experiments. *$p < 0.05$, **$p < 0.01$, ***$p < 0.001$,
602 ****$p < 0.001$ by two way ANOVA with Dunnett's multiple comparisons test (A) two way ANOVA with
603 Tukey's multiple comparisons test (M), Mann-Whitney test (B, H, K), one way ANOVA with Tukey's
604 multiple comparisons test (C, L), or multiple Mann-Whitney tests with Holm Sídák's multiple comparisons
605 test (D-G, I-J). ns, not significant. Graphs depict mean +/- SEM.
606

607 ***Tuft cell ACh regulates helminth clearance but not protist colonization***

608 There is little evidence to suggest that tuft cell sensing of *Tritrichomonas sp.* and
609 the resulting Type 2 immune response in the SI alter the total abundance of protists,[22]
610 but we wondered if tuft cell induced fluid secretion might instead regulate protist
611 localization along the length of the SI, with the goal of containing protists to the dSI and
612 cecum. We therefore assessed the abundance of protists across the pSI, dSI, and
613 cecum of vertically-colonized *Chat*$^{fl/fl}$*;Vil1-Cre* mice (Fig. S6A), hypothesizing an
614 increase of protists in the pSI of *Chat*-deficient mice. Constitutive deletion of *Chat* in tuft
615 cells had no effect on protist abundance or localization across the SI or cecum (Fig.
616 S6B). Treating protist-colonized mice with succinate to amplify Type 2 immunity also did
617 not uncover a phenotype (Fig. S6B), and acute deletion of *Chat* for 5 days likewise
618 failed to alter protist abundance or localization (Fig. S6C). Thus, the physiologic function
619 of protist sensing by tuft cells remains unclear.

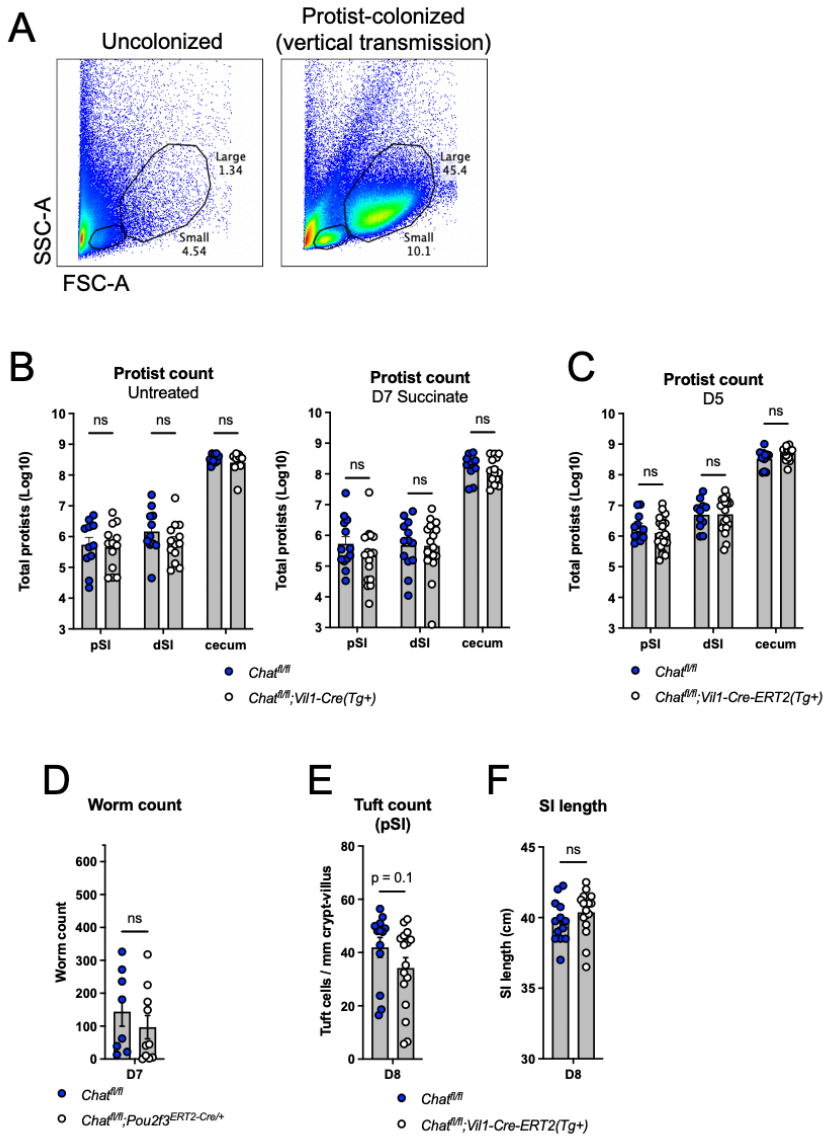

Supplemental Figure 6: (**A**) Representative flow cytometry of cecal contents from uncolonized and protist-colonized mice showing gating of protists by size. The "Large" gate contains *Tritrichomonas sp.* protists. (**B**) Quantification of total protists by flow cytometry in indicated tissues of vertically-colonized mice of indicated genotypes left untreated or given 150 mM Na_2-succinate in drinking water for 7 days. (**C**) Quantification of total protists by flow cytometry in indicated tissues of vertically-colonized mice of indicated genotypes administered tamoxifen 5 days prior to analysis. (**D**) Quantification of total SI *Nb* in mice of indicated genotype infected with *Nb* for 7 days without tamoxifen administration. (**E** and **F**) (E) Quantification of tuft cells (DCLK1+) by immunofluorescence and (F) total SI length 8 days post *Nb* infection of mice of indicated genotype given a single dose of tamoxifen (125 mg/kg) on day 5. In the graphs, each symbol represents an individual mouse (one tissue or average of two) from two or more pooled experiments. *p < 0.05, **p < 0.01, ***p < 0.001, ****p < 0.001 by multiple Mann-Whitney tests with

632 Holm Sídák's multiple comparisons test (B-C) or Mann-Whitney test (D-F). ns, not significant. Graphs
633 depict mean +/- SEM.
634
635 On the other hand, the requirement for tuft cell sensing and downstream Type 2
636 immunity for clearing helminths from the SI is well established.[11,20,45] To test if tuft cell
637 ACh contributes to helminth clearance, despite not impacting ILC2 activation or tissue
638 remodeling, we assessed worm burden in mice lacking epithelial *Chat* at 7 dpi, a
639 timepoint when WT mice begin to clear worms from the SI. Indeed, both constitutive and
640 acute deletion of epithelial *Chat* led to an increased SI worm burden (Fig. 6A). Tuft-
641 specific *Chat* deletion using *Pou2f3-Cre-Ert2* led to the same clearance delay 7 dpi (Fig.
642 6B). Worm burdens were equivalent in CRE-positive and -negative mice 5 dpi,
643 suggesting normal colonization of the SI by *Nb* arriving from the lung. The delayed
644 clearance was also not due to the loss of one *Pou2f3* allele in *Chat*$^{fl/fl}$*;Pou2f3*$^{Cre\text{-}ERT2/+}$
645 mice as they cleared worms normally when not treated with tamoxifen (Fig. S6D). In
646 order allow initiation of type 2 remodeling to proceed normally and delete tuft cell ACh
647 only during worm clearance, we waited until 5 dpi to administer a single dose of
648 tamoxifen to *Chat*$^{fl/fl}$*;Vil1-Cre-ERT2* mice. Consistent with our earlier observation that
649 tamoxifen suppresses intestinal Type 2 immunity, worm clearance in WT mice was
650 delayed to day 8, but we again found a *Chat*-dependent delay in worm clearance
651 despite normal intestinal remodeling. (Fig. 6C, Fig. S6E-F). Thus, we propose that tuft-
652 cell derived ACh contributes to worm clearance by the induction of epithelial fluid
653 secretion.

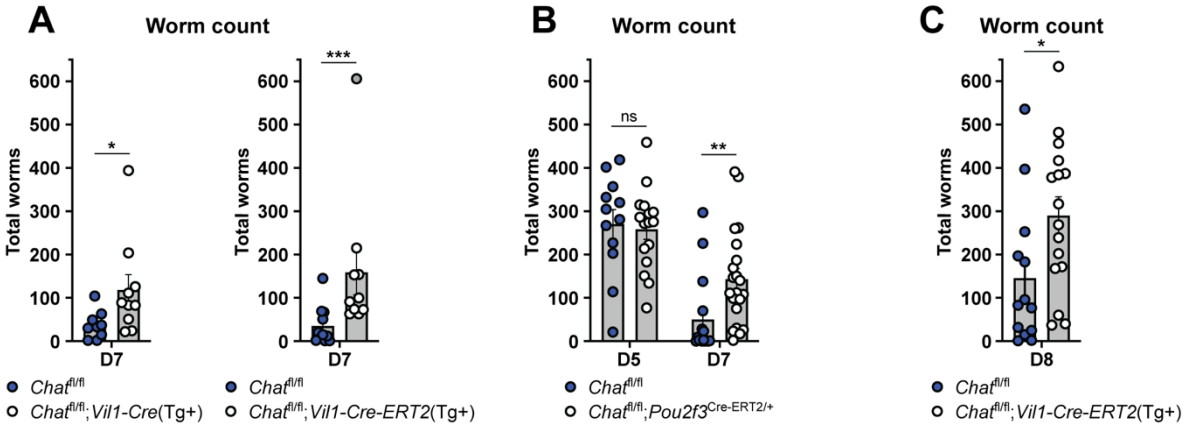

654
655 **Figure 6: Tuft cell-derived ACh contributes to helminth clearance.** (**A** and **B**) Quantification of total SI
656 *Nb* in mice of indicated genotypes at (A) 7 or (B) indicated days post infection. (**C**) Quantification of total

657 SI *Nb* 8 days post infection in mice of indicated genotypes given single dose of tamoxifen on D5. In the
658 graphs, each symbol represents an individual mouse pooled from two or more experiments. *p < 0.05,
659 **p < 0.01, ***p < 0.001, ****p < 0.001 by Mann-Whitney test (A, C), or multiple Mann-Whitney tests with
660 Holm Sídák's multiple comparisons test (B). ns, not significant. Graphs depict mean +/- SEM. Also see
661 Fig. S6.
662

663 **Discussion**

664 This study identifies an epithelium-intrinsic response unit that couples tuft cell
665 chemosensing to epithelial fluid secretion via the release of ACh from tuft cells. This
666 effector function is common to tuft cells in multiple tissues and is executed within
667 seconds of activation. In the SI, tuft cell-derived ACh is required for timely clearance of
668 helminth infection, but unlike all previously identified tuft cell effector functions, tuft cell-
669 derived ACh does not impact ILC2 activation nor downstream intestinal remodeling.
670 Instead, it appears that tuft cell ACh provides an acute signal that contributes to the
671 weep and sweep responses that push worms out of the intestine. The magnitude of tuft
672 cell-dependent fluid secretion correlates with the number of *Chat*+ tuft cells, suggesting
673 one possible function for the tuft cell hyperplasia that occurs even after initial sensing of
674 the helminth has been achieved.

675 Some details of tuft cell-regulated fluid secretion remain unresolved. For
676 example, we do not understand the regulation of *Chat* in SI tuft cells. It is unclear why
677 only a subset of SI tuft cells are *Chat*+, why there is a proximal to distal gradient of
678 *Chat*+ tuft cells, and why the frequency of *Chat*+ tuft cells decreases during Type 2
679 inflammation (although the total number increases due to tuft cell hyperplasia).
680 Furthermore, most tuft cells do not express *Slc5a7*, which encodes CHT1, the
681 transporter that neurons use to import choline for ACh synthesis, nor *Slc18a3*, which
682 encodes VAChT, a transporter that loads ACh into secretory vesicles in neurons.[70]
683 Lastly, it remains to be seen whether tuft cell-derived ACh also induces bicarbonate
684 secretion, as this often occurs together with chloride release and further supports the
685 unfolding of extracellular mucus.[71]

686 We have also not identified the precise ACh receptor(s) that mediate(s) the fluid
687 secretion response, although inhibition by atropine implicates a muscarinic rather than
688 nicotinic receptor. *Chrm1* and *Chrm3* are the only detectable muscarinic receptor

689 transcripts in unmanipulated SI epithelium[9,11] and *Nb* clearance is delayed in *Chrm3*$^{-/-}$
690 mice.[40] Induction of Type 2 cytokines is also impaired in these *Chrm3*$^{-/-}$ mice, so
691 conditional *Chrm* alleles will be needed to identify in which cells the receptors are
692 required and for which aspects of Type 2 immunity.
693 While tuft cell-derived ACh was not required for ILC2 activation during helminth
694 infection and intestinal remodeling was largely intact, there were slight yet significant
695 defects in tuft cell numbers or SI length at some timepoints analyzed. Prior literature has
696 shown that deletion of *Chrm3* from the SI epithelium causes an *increase* in tuft cell
697 numbers at baseline but a *decrease* in tuft cells following irradiation.[67] Perhaps epithelial
698 ACh signaling has damage-induced functions that overlap with helminth-induced
699 intestinal remodeling. Regulation of intestinal epithelial differentiation by tuft cell-derived
700 ACh bears further study.
701 We have focused on tuft cell ACh signaling on enterocytes to drive fluid
702 secretion, but ACh receptors are expressed by many cells, including other types of
703 intestinal epithelial cells. Goblet cells undergo compound exocytosis of mucus in
704 response to ACh,[46,47,72] and the formation of goblet-associated antigen passages
705 (GAPs) has also been linked to ACh signaling.[73,74] Additionally, tuft cell ACh was
706 recently reported to induce mucus secretion from cholangiocytes in the gallbladder.[57]
707 We therefore extensively tested the hypothesis that ACh from SI tuft cells signals on
708 villus goblet cells to induce mucus secretion and GAP formation, but we could not find
709 any evidence that this occurs *in vivo* (data not shown). A recent study demonstrating
710 that muscarinic receptor expression is restricted to GCs at the base of SI crypts, and
711 that only these cells respond acutely to CCh,[75] may explain why we did not detect tuft
712 cell-dependent regulation of GC mucus secretion. While it remains possible that ACh
713 from SI crypt tuft cells regulates secretion by GCs (and Paneth cells), we generally
714 found fewer *Chat*+ tuft cells in the crypts than in the villi, and chemosensing pathways
715 are likely not yet functional in immature crypt tuft cells. Perhaps in the colon tuft cell
716 ACh regulates the function of sentinel GCs at crypt openings.[76] Lastly, ACh-regulated
717 smooth muscle contraction is critical for SI helminth clearance[28,37] and tuft cells have
718 been linked to smooth muscle function in other tissues.[19,57] The short extracellular half-
719 life of ACh combined with the distance between epithelial tuft cells and smooth muscles

720 that surround the SI make direct signaling unlikely. Nonetheless, while we did not see
721 evidence of direct contact between tuft cells and enteric neurons, they have been
722 previously reported in the SI[10,77,78] and thus we cannot rule out the possibility that tuft
723 cell ACh regulates smooth muscle contraction via the enteric nervous system.
724 During Type 2 inflammation in the SI, the maximal fluid secretion induced by ACh
725 is dramatically reduced,[69] possibly to prevent excessive fluid loss or diarrhea during
726 chronic helminth infection. At the same time, the number of *Chat*+ tuft cells increases,
727 such that tuft cell-regulated fluid secretion is maintained or even enhanced compared to
728 baseline. This re-wiring of ACh-regulated fluid secretion may represent a regulatory
729 mechanism that minimizes fluid loss due to endogenous signals while maintaining the
730 ability to respond to lumen-restricted agonists such as helminths via tuft cell sensing. In
731 that regard, tuft cells also have an advantage over mast cells and neurons, which can
732 induce enhanced fluid secretion during Type 2 inflammation via release of histamine
733 and/or prostaglandin E2,[69] but can only respond to ligands that penetrate the mucosal
734 barrier. Relatedly, it remains unclear whether the acetylcholinesterases secreted by
735 helminths can penetrate the mucosal barrier to target ACh in the tissue, or whether
736 helminths are only able to counter the effects of ACh during tissue-dwelling phases of
737 their lifecycle.
738 Although we have focused on the SI in this study, we propose tuft cells link
739 chemosensing to fluid secretion in all tissues. Indeed, with the exception of tuft-ILC2
740 circuit activation, all other known tuft cell effector functions occur instantaneously and
741 seem to mediate evasion (e.g. breathing cessation)[14,16] and expulsion (e.g. mucociliary
742 sweep) of microbes and other agonists.[8,17] Fluid secretion fits this paradigm. The
743 mucosal barrier must be constantly hydrated and fluid secretion can provide a flushing
744 effect. Based on the ligands tuft cells sense in different tissues, such mechanisms could
745 be important to clear allergens from the upper airways or bacteria from the trachea and
746 urethra. Tuft cell sensing may also reduce baseline fluid secretion, as one recent study
747 suggested.[79] The ligands and function of tuft cells in the colon are only just being
748 elucidated,[56] but we predict that tuft cell-regulated fluid secretion would help maintain a
749 healthy mucosal barrier here too. Tuft cell frequency is generally decreased in patients
750 with active inflammatory bowel disease,[80,81] consistent with a role for tuft cells in

751 preventing bacterial infiltration. Conversely, increased tuft cell frequency was detected
752 in colonic biopsies from patients with diarrhea-predominant irritable bowel syndrome, a
753 largely non-inflammatory condition of unknown origin.[82]
754 Why tuft cells sense succinate in either the SI or, as we have now demonstrated,
755 the trachea, remains unclear. We could not find any impact of tuft cell *Chat* deletion on
756 *Tritrichomonas* burden or distribution, but perhaps tuft cell-mediated fluid secretion,
757 together with IL-13-induced anti-microbial peptides and mucus production, acts more
758 locally to keep microbes away from the epithelium.[83] Succinate levels have also been
759 shown to increase in contexts of bacterial dysbiosis, and inducing tuft cell hyperplasia
760 with succinate treatment reduces inflammation in a model of ileitis.[80] As for the trachea,
761 aberrant release of cellular succinate into the airways, which occurs in some patients
762 with cystic fibrosis, can promote colonization and biofilm formation by the
763 pathosymbiont *Pseudomonas aeruginosa*.[84] Induction of CFTR-dependent fluid
764 secretion by prostaglandin E2 released from airway tuft cells has also been
765 suggested.[86] Thus, tracheal tuft cells may induce fluid secretion to flush away succinate
766 and other soluble molecules and to deter bacterial accumulation.
767 Therapeutically, benefit may be achieved by tuning tuft cell effector functions up
768 or down, depending on the context and need. For example, tuft cell-induced fluid
769 secretion may prove useful in treating cystic fibrosis patients in whom CFTR-dependent
770 fluid secretion is impaired, while certain patients suffering from diarrhea might benefit
771 from reduced tuft cell function. Future study should investigate the involvement of tuft
772 cell-induced fluid secretion in human disease.
773
774 **Acknowledgements:**

775 We thank all members of the von Moltke lab for helpful discussion and input on this
776 manuscript. We thank D. Hailey and the Garvey Cell Imaging Lab in the Institute for
777 Stem Cell & Regenerative Medicine for microscopy support; the mouse husbandry staff
778 in the UW SLU vivarium; V. Gersuk, K. O'Brien and the Benaroya Research Institute
779 Genomics Core for help with RNA sequencing; and M. F. Fontana for helpful comments
780 on the manuscript. Flow cytometry data were acquired through the University of

Washington, Cell Analysis Facility Shared Resource Lab, with NIH award 1S10OD024979-01A1 funding for the Symphony A3. We thank Takeda for the generous gift of the Class 8 TRPM5 agonist.

Funding

TEB was supported by the UW Immunology Fellowship, and DLJ was a UW Mary Gates scholar. MMM is a Hannah H. Gray fellow and JvM is a Searle Scholar and a Burroughs Wellcome Investigator in the Pathogenesis of Infectious Disease. Work at the University of Washington was supported by NIH DP2OD024087, R01AI145848, and R01AI167923. Work at Stanford was supported by NIH R01DK128292 and R21AI171222 (MRH). CF is an A.P. Giannini Fellow and was also supported by the Stanford School of Medicine Dean's Postdoctoral Fellowship and Stanford Maternal & Child Health Research Institute Postdoctoral Fellowship. Work at Seattle Children's Research Institute was supported by NIH R01HL128361 (JSD) and K24AI150991 (JSD).

Contributions:

TEB designed and performed experiments, analyzed data, and wrote the paper with JVM. LMW, DBS, MMM, DNK, and JWM assisted with experiments at the University of Washington. CF and MBG performed *in vivo* Class 8 and *T. musculis* fecal water content experiments at Stanford University with supervision and funding provided by MRH. KAB and LMR performed pilot Ussing chamber experiments with supervision and funding provided by JSD. AB, MS, and RM led the development and validation of the Class 8 TRPM5 agonist at Takeda Pharmaceuticals in collaboration with Evotec. JVM conceived of and supervised the study, analyzed data, acquired funding, and wrote the paper with TEB.

Methods:

Study Design

808 All experiments were performed using randomly assigned mice without investigator
809 blinding. No data were excluded, except from Ussing chambers when mounted tissues
810 failed to respond to stimulation by a positive control (e.g. CCh). All data points reflect
811 biological replicates, except for *in vitro* ILC2 stimulations and epithelial monolayer
812 experiments where each data point is a technical replicate. Data were pooled from
813 multiple experiments unless otherwise noted. The number of independent experiments
814 is included in the figure legends.

815 **Experimental Animals**

816 Mice aged 6 weeks and older were used for all experiments. Mice were age-matched
817 within each experiment. Pooled results include both male and female mice of varying
818 ages unless otherwise indicated. Mouse strains used in this study are listed in Table S3.
819 Acute deletion of conditional alleles in mice was achieved by oral gavage with tamoxifen
820 dissolved in corn oil (100 mg/kg). *Chat*$^{fl/fl}$*;Vil1-Cre-ERT2(Tg+)* mice were administered
821 tamoxifen on day -4 and 0 of infection with *N. brasiliensis* and on day -6 and -4 of
822 treatment with 150 mM succinate drinking water, or as noted in the text.
823 *Chat*$^{fl/fl}$*;Pou2f3*$^{Cre\text{-}ERT2/+}$ mice were administered tamoxifen every other day starting on
824 day -4 of *N. brasiliensis* infection or as noted in the text. *DREADD(Tg+); Pou2f3*$^{Cre\text{-}ERT2/+}$
825 mice were administered tamoxifen chow for 7 days prior to Ussing experiments. All mice
826 (CRE+ and CRE-) received tamoxifen treatment. All mice were maintained in specific
827 pathogen-free conditions at the University of Washington or Stanford University and
828 were confirmed to be free of *Tritrichomonas sp.* by microscopy and qPCR, unless
829 specifically colonized for experimental purposes. All procedures were conducted within
830 University of Washington or Stanford University (Class 8 gavage) IACUC guidelines
831 under approved protocols.
832

833 **Measuring epithelial ion flux with Ussing chambers**

834 Ussing chamber protocols were informed by Clarke et al.[51]
835

836 *Tissue mounting*: Mice 7-12 weeks of age were euthanized by CO_2 and segments of the
837 intestine (SI, cecum, colon) were harvested and flushed with cold Krebs Buffered

838 Ringer's solution + mannitol (10 mM D-mannitol, 115 mM NaCl, 2.4 mM K_2HPO_4, 0.4
839 mM KH_2PO_4, 25 mM $NaHCO_3$, 1.2 mM $CaCl_2$ dihydrate, 1.2 $MgCl_2$ hexahydrate; pH
840 7.25-7.4). Intestines (first 5 cm of pSI and last 5 cm of dSI) were fileted open along the
841 mesenteric line, trimmed and mounted to the pins of an Ussing chamber cassette with
842 aperture of 0.3 cm^2 (Physiologic Instruments, Reno, USA), avoiding Peyer's patches.
843 For some experiments the SI was pinned to a Sylgard-coated plate with the serosal side
844 up and the muscle layer scored with a scalpel and "stripped" away using forceps under
845 a dissection scope. The resulting epithelium-submucosa tissue was mounted in a
846 cassette as normal. For trachea preparations, the entire trachea was harvested,
847 surrounding tissue (esophagus) removed, and cut open lengthwise along the anterior
848 side (away from esophagus) for mounting in a 2 mm^2 aperture cassette (Physiologic
849 Instruments, Reno, USA). Cassettes containing tissues were mounted in Ussing
850 chambers (Physiologic Instruments, Reno, USA) and the lumenal chambers filled with 5
851 mL of KBR + mannitol and the basolateral chambers filled with 5 mL of KBR + glucose
852 (10 mM D-glucose, 115 mM NaCl, 2.4 mM K_2HPO_4, 0.4 mM KH_2PO_4, 25 mM $NaHCO_3$,
853 1.2 mM $CaCl_2$ dihydrate, 1.2 $MgCl_2$ hexahydrate; pH 7.25-7.4). The chambers were
854 warmed to 37C and bubbled with carbogen (95% O_2, 5% CO_2) for the duration of the
855 experiment. For Cl^- replacement experiments, Cl^- free KBR was used, in which
856 gluconate is substituted for Cl- (115 mM D-gluconic acid sodium salt, 2.4 mM K_2HPO_4,
857 0.4 mM KH_2PO_4, 25 mM $NaHCO_3$, 4 mM calcium D-gluconate monohydrate, 1.2 mM
858 magnesium D-gluconate hydrate; pH 7.25-7.4).
859
860 *Measuring the short circuit current (Isc)*: Automatic voltage clamping was performed by
861 MultiChannel Voltage-Current Clamp (Physiologic Instruments, Reno, USA). Voltage
862 differences between electrodes and fluid resistance of the buffer were compensated
863 prior to insertion of the tissue cassette. Isc was measured by voltage clamp every 1
864 second and recorded using Acquire & Analyze software (Physiologic Instruments, Reno,
865 USA) and normalized to tissue area. After a 20 min equilibration period, tissues were
866 stimulated lumenally with Na_2-succinate (1, 10 mM) or cis-epoxysuccinic acid (10 mM),
867 basolaterally with 5 μM Class 8, or bilaterally with 1 μM Compound 21. For
868 succinate/cESA stimulation, subsequent stimulations were administered every 10 min;

869 for Class 8 the interval was increased to 15 min due to the slower kinetics of the
870 response. Subsequent stimulations included lumenal 20 mM NaCl, basolateral 100 μM
871 CCh, and bilateral cocktail of 100 μM 3-Isobutyl-1-methylxanthine (IBMX) + 10 μM
872 forskolin. Chemical inhibitors were administered 5 min after start of equilibration period
873 (15 min before first stimulation): basolateral 100 μM bumetanide, bilateral 10 μM
874 ibuprofen, basolateral 10 μM atropine, basolateral 1 μM tetrodotoxin, and lumenal 1 mM
875 carbenoxolone. ΔIsc values were calculated as the difference between the Isc
876 measurement at the peak of the stim response and the Isc measurement taken right
877 before adding the agonist. For tissues that did not respond to the agonist (e.g., knockout
878 mouse intestines, tissues treated with inhibitors) and therefore had no peak response,
879 the Isc value was taken at the same timepoint as the peak Isc value for the
880 corresponding WT or control tissue.
881
882 **Measuring fecal water content**
883 Mice were orally gavaged with vehicle (0.5% methylcellulose + 1% Tween 20) or 30
884 mg/kg Class 8, and fecal samples (2+ pellets) were taken at 0 and 3 hours post gavage.
885 For protist-colonized experiments, B6 mice were colonized with *T. musculis* protists and
886 fecal samples collected at 2, 7,14, and 20 days post colonization. Fecal samples were
887 dried at 60C overnight and % water content calculated as (1-(dry weight/wet
888 weight))*100.
889
890 **Monolayer culture and cysteinyl leukotriene ELISA**
891 Proximal small intestine was isolated and villi were gently scraped off with a glass
892 coverslip. Tissue was incubated for 30 minutes at 4° with 2mM EDTA to release
893 epithelial crypts, then washed twice with cold PBS and filtered through a 70 um strainer.
894 Crypts were resuspended in complete monolayer media (DMEM/F12 supplemented
895 with 2mM glutamine, 100U/mL penicillin, 100mg/mL streptomycin, 10mM HEPES, N2
896 supplement, B27 supplement, R-spondin (10% supernatants from R-spondin secreting
897 cells), Noggin (10% supernatant from Noggin secreting cells), 500mM N-acetylcysteine,
898 50ug/mL mEGF, and 10 μM Y27632). Plates were coated with 2% Matrigel in cold
899 DMEM/F12 and incubated at 37° for at least 30 minutes. Media was aspirated from the

900 plate, and 1000 crypts were plated per well of a 48-well plate. Crypts were incubated
901 overnight, and non-adherent cells were aspirated the next day. Test stimuli diluted in
902 HBSS containing Ca2+/Mg2+ were added to monolayers and stimulated at 37° for 30
903 minutes. Supernatants were collected and used for the Cysteinyl Leukotriene Express
904 ELISA kit (Cayman Chemical) according to manufacturer's protocol.
905
906 **Succinate and cytokine treatment**
907 For succinate experiments mice were given 150mM sodium succinate hexahydrate
908 (Thermo) ad libitum in drinking water for the indicated amount of time. Recombinant
909 murine IL-25 (500 ng; R&D) was given for 3 consecutive days intraperitoneally in 200 µL
910 PBS.
911
912 **Helminth infections and analysis**
913 *N. brasiliensis* larvae were raised and maintained as previously described.[85]
914 Mice were infected subcutaneously with 500 *N. brasiliensis* L3. At sacrifice, the entire SI
915 was fileted open and total worms counted under a stereomicroscope.
916
917 **Protist colonization and analysis**
918 Breeding pairs were colonized with *Tritrichomonas musculis* or *T. rainier* as previously
919 described.[87] Pups from colonized breeding pairs were analyzed. Protist numbers were
920 quantified by flow cytometry as described by Chudnovskiy et al.[88] Briefly, 10 cm of pSI
921 and dSI were flushed into a 15 mL conical with 10 mL RT PBS using a gavage needle.
922 Cecal contents were harvested into 15 mL conical, weighed, and then 10 mL RT PBS
923 added. Samples were let sit for 30 min at RT, vortexed, and then passed through a 70
924 µm filter. Protists were washed, stained with DAPI, then count beads added and data
925 collected on a FACSCanto II (BD Biosciences). Protist numbers per gram of cecal
926 content was calculated.
927
928 **Intestinal tissue fixation and staining**
929 Intestinal tissues were flushed with PBS and fixed in 4% paraformaldehyde for 3-4
930 hours at 4°C, washed with PBS, and incubated in 30% (w/v) sucrose overnight at 4°C.

931 Samples were then coiled into “Swiss rolls”, embedded in Optimal Cutting Temperature
932 Compound (Tissue-Tek) and sectioned at 8 μm on a CM1950 cryostat (Leica).
933 Immunofluorescent staining was performed in PBS with 1% BSA at room temperature
934 as follows: 1 hr 10% donkey serum with 1:1000 Fc Block, 1 hr (or O/N at 4°C) primary
935 antibody, 5 min wash, 45 min secondary donkey antibody and/or WGA-488, 5 min
936 wash, and mounted with Vectashield plus DAPI (Vector Laboratories). Images were
937 acquired with an Axio Observer A1 (Zeiss) microscope with a 10X or 20X A Plan
938 objective. Tuft cell frequency was calculated using ImageJ software to manually quantify
939 DCLK1^{+} cells per millimeter of crypt-villus axis. Goblet cell frequency was calculated
940 using ImageJ software to manually quantify total WGA+ cells in the villus (crypts were
941 excluded because WGA also labels Paneth cells) per millimeter of crypt villus axis. For
942 each replicate, four 10x images of the Swiss roll were analyzed and at least 25 total villi
943 counted.
944
945 **Single-cell tissue preparation for flow cytometry**
946 For single cell epithelial preparations from SI, tissues were flushed with PBS,
947 Peyer’s patches removed, opened longitudinally, and rinsed with PBS. Tissue was cut
948 into small pieces, shaken vigorously for 20 seconds in 30 mL cold HBSS (Ca^{+2}/Mg^{+2}-
949 free) with 1 mM HEPES, drained, and then incubated rocking at 37°C for 10 min in 15
950 mL HBSS (Ca^{+2}/Mg^{+2}-free) supplemented with 3 mM EDTA and 1 mM HEPES. Tissues
951 were vortexed thoroughly and released epithelial cells passed through a 70 μm filter.
952 This process was repeated for a total of 3 rounds. Supernatants were pooled and
953 washed with HBSS (Ca^{+2}/Mg^{+2}-free) with 1 mM HEPES before staining for flow
954 cytometry.
955 For lamina propria (LP) preparations from uninfected mice, SI was processed as
956 above to remove the epithelial fraction. Tissues were then incubated shaking at 37°C for
957 30 minutes in 10 mL RPMI 1640 supplemented with 20% FCS, 1 mM HEPES, 0.05
958 mg/ml DNase I (Sigma Aldrich), and 1 mg/mL Collagenase A (Sigma Aldrich). Tissues
959 were vortexed and cells were passed through a 100 μm filter, then a 40 μm filter,
960 washing with cold HBSS (Ca^{+2}/Mg^{+2}-free) with 1 mM HEPES. Cells were washed and
961 stained for flow cytometry.

962 For LP preparations from *N. brasiliensis*-infected mice (D4), mice were
963 anaesthetized with 5% avertin. The peritoneal cavity was opened, the SI nicked at the
964 junction with the stomach and transected at the cecum and flushed with 20 mL of 37°C
965 HBSS (Ca^{+2}/Mg^{+2}-free) plus 1 mM HEPES. Then the mice were perfused through the
966 heart with 30 mL of 37°C HBSS (Ca^{+2}/Mg^{+2}-free) with 30 mM EDTA and 1 mM HEPES.
967 Three minutes after perfusion was completed, the first 10 cm of the proximal SI was
968 harvested, Peyer's patches removed, opened longitudinally, and cut into small pieces
969 and shaken vigorously for 20 seconds in 30 mL cold HBSS (Ca^{+2}/Mg^{+2}-free) with 1 mM
970 HEPES, then drained. Tissues were then digested and processed as above in
971 uninfected mice.
972 For mesenteric lymph node (MLN) preparations, SI-draining MLN were harvested
973 into RPMI + 5% FBS on ice, mashed through a 70 μm filter, the filter washed with RPMI
974 + 5% FBS, and cells washed and stained for flow cytometry.
975
976 **Flow cytometry and cell sorting**
977 Single cell suspensions from tissues were prepared as described above. For flow
978 cytometry, SI epithelium and MLN samples were stained in DPBS (Ca^{+2}/Mg^{+2}-free) with
979 3% FCS and LP samples were stained in PBS (Ca^{+2}/Mg^{+2}-free) with 3% FCS, 2 mM
980 EDTA, and 0.02 mg/mL DNase I with antibodies to surface markers for 30 min at 4°C,
981 followed by DAPI (Roche) for dead cell exclusion. When cell counts were needed,
982 counting beads (Spherotech) were added prior to running flow cytometry. Samples were
983 run on a FACSCanto II or LSRII (BD Biosciences) and analyzed with FlowJo 10.8.1.
984 Samples were FSC-A/SSC-A gated to exclude debris, FSC-A/FSC-H gated to select
985 single cells, and gated to exclude dead cells. For cell sorting, single cell suspensions
986 were prepared and stained as described and sorted on an Aria III (BD Biosciences).
987
988 **ILC2 Stimulation Assay**
989 Entire SILP from several mice were pooled and ILC2s (EpCAM-, $CD45^{+}$, Lin(CD3, CD4,
990 CD5, CD8, CD11b, CD19, NK1.1, FcER1)$^{-}$, $KLRG1^{+}$) sorted as described. Sorted cells
991 were plated at 5000 cells per well in a 96-well plate and incubated at 37°C overnight in
992 10 ng/ml IL-7 (R&D Systems) and basal media composed of high glucose DMEM

993 supplemented with non-essential amino acids, 10% FBS, 100 U/mL penicillin,
994 100mg/mL streptomycin, 10mM HEPES, 1mM sodium pyruvate, 100μM 2-
995 mercaptoethanol, and 2mM L-glutamine. The next morning, media was replaced and
996 cells were stimulated with the indicated agonist. After a six-hour stimulation,
997 supernatant was collected and the cells were washed and stained with 1 uL/well of PE-
998 conjugated anti-human CD4 for 20 min at 4°C. Cells were washed, resuspended in
999 DAPI and analyzed on a CantoRUO (BD Biosciences). Cytokine levels in supernatants
1000 were measured using Enhanced Sensitivity Flex Sets (BD Biosciences) for mouse IL-5
1001 and IL-13 according to the manufacturer's protocol. Data was collected on an LSRII (BD
1002 Biosciences).
1003
1004 **RNA Sequencing and Analysis**
1005 150-200 tuft cells were sorted directly into lysis buffer from the SMART-Seq v4 Ultra
1006 Low Input RNA Kit (Takara) and cDNA generated following manufacturer's instructions.
1007 Cells were sorted from four individual mice for each experiment. Sequencing libraries
1008 were generated using the Nextera XT library preparation kit with multiplexing primers,
1009 according to manufacturer's protocol (Illumina), and library quality assessed using
1010 Tapestation (Agilent). High throughput sequencing was performed on NextSeq 2000
1011 (Illumina), sequencing dual-indexed and paired-end 59 base pair reads. All samples
1012 were in the same run with a target depth of 5 million reads. Base calls were processed
1013 to FASTQs on BaseSpace (Illumina), and a base call quality-trimming step was applied
1014 to remove low-confidence base calls from the ends of reads. The FASTQs were aligned
1015 to the GRCm38 mouse reference genome, using STAR v.2.4.2a and gene counts were
1016 generated using htseq-count. Further analysis of the data was performed using the
1017 DIY.Transcriptomics (diytranscriptomics.com) pipeline, with experiment-specific
1018 modifications. Samples were filtered to exclude genes with counts per million = 0 in 4 or
1019 more samples and genes annotated as pseudogenes. Finally, samples were normalized
1020 to each other. To identify differentially expressed genes, precision weights were first
1021 applied to each gene based on its mean-variance relationship using VOOM,[89] then data
1022 was normalized using the TMM method[90] in EdgeR.[91] Linear modeling and bayesian
1023 stats were employed via Limma[92] to find genes that were up- or down-regulated by 2-

1024 fold (Log2FC = 1) or more, with a false-discovery rate (FDR) of 0.01. The code and
1025 results for these analyses are included as Data File S1 and S2.
1026
1027 **Statistical Analysis**
1028 Statistical analysis was performed as noted in figure legends using Prism 9 (GraphPad)
1029 software. Graphs show mean +/- SEM.
1030

1031 **Table S3**

Reagent or Resource	Source	Identifier
B6.Cg-Tg(RP23-268L19-EGFP)2Mik/J (Chat-GFP)	Jackson Laboratory	JAX #007902
B6.*Il25*$^{Flare25/Flare25}$ (Il25-RFP)	R. Locksley (PMID: 26675736)	NA
B6.*Il13*$^{Smart13/Smart13}$ (Smart13)	R. Locksley (PMID: 22138715)	NA
C57BL/6N-Pou2f3<tm1(KOMP)Vlcg>/Tcp (*Pou2f3*$^{-/-}$)	Canadian Mouse Mutant Repository	CMMR #ABDF
B6.129P2-Trpm5^{tm1Dgen}/J (Trpm5$^{-/-}$)	Jackson Laboratory	JAX #005848
B6.*Sucnr1*$^{-/-}$	In-house (PMID: 30021144)	NA
B6.*Il25*$^{-/-}$	A. McKenzie (PMID: 16606668)	NA
B6;129-Chat^{tm1Jrs}/J (*Chat*$^{fl/fl}$)	Jackson Laboratory	JAX #016920
B6.Cg-Tg(Vil1-cre)997Gum/J	Jackson Laboratory	JAX #004586
B6.Cg-Tg(Vil1-cre)1000Gum/J (Vil1-Cre1000)	Jackson Laboratory	JAX #021504
B6.Cg-Tg(Vil1-cre/ERT2)23Syr/J (*Vil1-Cre-Ert2*)	Jackson Laboratory	JAX #020282
B6(129S4)-*Pou2f3*$^{tm1.1(cre/ERT2)Imt}$/J (Pou2f3-Cre-Ert2)	Jackson Laboratory	JAX #037511
B6.129S-Chattm1(cre)Lowl/MwarJ (*Chat-Cre*)	Jackson Laboratory	JAX #031661
B6.*Il25-Cre*	R. Locksley (PMID: 35245089)	NA
B6.Cg-*Gt(ROSA)26Sor*$^{tm9(CAG-tdTomato)Hze}$/J (Ai9)	Jackson Laboratory	JAX #007909
B6N;129-Tg(CAG-CHRM3*,-mCitrine)1Ute/J (Gq-DREADD)	Jackson Laboratory	JAX #026220
B6.129-*Gt(ROSA)26Sor*$^{tm1(CAG-CHRM4*,-mCitrine)Ute}$/J (Gi-DREADD)	Jackson Laboratory	JAX #026219
B6.*Alox5*$^{fl/fl}$	In-house (PMID: 32160525)	NA
B6.*Il4ra*$^{fl/fl}$	F. Brombacher (PMID: 15142530)	NA

1032

1033 **Table S4**

Reagent or Resource	Dilution Factor	Source	Identifier
Rabbit α-DCLK1	1:1000	Abcam	Cat#ab31704
Rabbit α-TUJ1 (Beta-III tubulin)	1:500	Abcam	Cat#ab18207
Goat α-GFP	1:500	Novus Bio	Cat#NB100-1770
Rabbit α-dsRed	1:500	Clontech	Cat#632496
Rabbit α-HA, clone 16B12	1:1000	Biolegend	Cat#901516
WGA-488	1:150	Thermo	Cat#W11261
Donkey α-Rabbit IgG AF594	1:1000	Thermo	Cat#A-21207
Donkey α-Goat IgG AF488	1:500	Thermo	Cat#A-11055
CD16 / CD32, clone 2.4G2	1:1000	Tonbo	Cat# 70-0161-M001
CD3 PerCP-Cy5.5, clone 145-2C11	1:100	Biolegend	Cat#100328
CD3 BV421, clone 145-2C11	1:400	Biolegend	Cat#100335
CD4 BV711, clone RM4-5	1:250	Biolegend	Cat#100549
CD4 eF450, clone RM4-5	1:200	eBioscience	Cat# 48-0042-80
hCD4 PE, clone RPA-T4	1:50	Biolegend	Cat#300508
CD5 PerCP-Cy5.5, clone 53-7.3	1:500	Biolegend	Cat#100624
CD5 eF450, clone 53-7.3	1:400	Biolegend	Cat#100607
CD8 PerCP-Cy5.5, clone 53-6.7	1:200	Biolegend	Cat#100724
CD8 BV421, clone 53-6.7	1:400	Biolegend	Cat#100737
CD11b AF700, clone M1/70	1:250	Biolegend	Cat#101222
CD11b BV421, clone M1/70	1:400	Biolegend	Cat# 101235
CD19 PerCP-Cy5.5, clone 6D5	1:250	Biolegend	Cat#115533
CD19 BV421, clone 6D5	1:400	Biolegend	Cat# 115537

CD24 PE, clone M1/69	1:300	Biolegend	Cat#101807
CD24 PerCP-Cy5.5, clone M1/69	1:300	Biolegend	Cat#101824
CD45 BV605, clone 30F11	1:300	Biolegend	Cat#103155
CD45 BV650, clone 30F11	1:500	Biolegend	Cat#103151
EpCAM PE-Dazzle, clone G8.8	1:300	Biolegend	Cat#118235
EpCAM AF488, clone G8.8	1:300	Biolegend	Cat#118210
EpCAM PE-Cy7, clone G8.8	1:300	Biolegend	Cat#118215
FcER1 BV421, clone Mar-1	1:400	Biolegend	Cat#334623
IL17RB APC, clone 9B10	1:100	Biolegend	Cat#146307
KLRG1 PE-Cy7, clone 2F1	1:250	Biolegend	Cat#138416
NK1.1 PerCP-Cy5.5, clone PK136	1:100	Biolegend	Cat#108728
NK1.1 BV421, clone PK136	1:200	Biolegend	Cat#108731
Siglec-F APC-Cy7, clone E50-2440	1:100	BD	Cat#565527
Siglec-F AF647, clone E50-2440	1:100	BD	Cat# 562680
Thy1.2 (CD90.2) BV605, clone 53-2.1	1:500	Biolegend	Cat#140318

1034
1035
1036
1037
1038

1039 **References**

1040 1. Frizzell, R.A., and Hanrahan, J.W. (2012). Physiology of epithelial chloride and fluid
1041 secretion. Cold Spring Harb Perspect Med *2*, a009563.
1042 10.1101/cshperspect.a009563.

1043 2. Cooke, H.J. (1998). “Enteric Tears”: Chloride Secretion and Its Neural Regulation.
1044 News Physiol Sci *13*, 269–274.

1045 3. Xue, J., Askwith, C., Javed, N.H., and Cooke, H.J. (2007). Autonomic nervous system
1046 and secretion across the intestinal mucosal surface. Auton Neurosci *133*, 55–63.
1047 10.1016/j.autneu.2007.02.001.

1048 4. Hirota, C.L., and McKay, D.M. (2006). Cholinergic regulation of epithelial ion transport
1049 in the mammalian intestine. Br J Pharmacol *149*, 463–479. 10.1038/sj.bjp.0706889.

1050 5. Cox, M.A., Bassi, C., Saunders, M.E., Nechanitzky, R., Morgado-Palacin, I., Zheng,
1051 C., and Mak, T.W. (2020). Beyond neurotransmission: acetylcholine in immunity and
1052 inflammation. J Intern Med *287*, 120–133. 10.1111/joim.13006.

1053 6. Mashimo, M., Moriwaki, Y., Misawa, H., Kawashima, K., and Fujii, T. (2021).
1054 Regulation of Immune Functions by Non-Neuronal Acetylcholine (ACh) via
1055 Muscarinic and Nicotinic ACh Receptors. Int J Mol Sci *22*, 6818.
1056 10.3390/ijms22136818.

1057 7. Yajima, T., Inoue, R., Matsumoto, M., and Yajima, M. (2011). Non-neuronal release
1058 of ACh plays a key role in secretory response to luminal propionate in rat colon. J
1059 Physiol *589*, 953–962. 10.1113/jphysiol.2010.199976.

1060 8. Perniss, A., Liu, S., Boonen, B., Keshavarz, M., Ruppert, A.-L., Timm, T., Pfeil, U.,
1061 Soultanova, A., Kusumakshi, S., Delventhal, L., et al. (2020). Chemosensory Cell-
1062 Derived Acetylcholine Drives Tracheal Mucociliary Clearance in Response to
1063 Virulence-Associated Formyl Peptides. Immunity *52*, 683-699.e11.
1064 10.1016/j.immuni.2020.03.005.

1065 9. Haber, A.L., Biton, M., Rogel, N., Herbst, R.H., Shekhar, K., Smillie, C., Burgin, G.,
1066 Delorey, T.M., Howitt, M.R., Katz, Y., et al. (2017). A single-cell survey of the small
1067 intestinal epithelium. Nature *551*, 333–339. 10.1038/nature24489.

1068 10. Bezençon, C., Fürholz, A., Raymond, F., Mansourian, R., Métairon, S., Le
1069 Coutre, J., and Damak, S. (2008). Murine intestinal cells expressing Trpm5 are
1070 mostly brush cells and express markers of neuronal and inflammatory cells. J Comp
1071 Neurol *509*, 514–525. 10.1002/cne.21768.

1072 11. Nadjsombati, M.S., McGinty, J.W., Lyons-Cohen, M.R., Jaffe, J.B., DiPeso, L.,
1073 Schneider, C., Miller, C.N., Pollack, J.L., Nagana Gowda, G.A., Fontana, M.F., et al.
1074 (2018). Detection of Succinate by Intestinal Tuft Cells Triggers a Type 2 Innate
1075 Immune Circuit. Immunity *49*, 33-41.e7. 10.1016/j.immuni.2018.06.016.

1076 12. Schütz, B., Ruppert, A.-L., Strobel, O., Lazarus, M., Urade, Y., Büchler, M.W.,
1077 and Weihe, E. (2019). Distribution pattern and molecular signature of cholinergic tuft
1078 cells in human gastro-intestinal and pancreatic-biliary tract. Sci Rep *9*, 17466.
1079 10.1038/s41598-019-53997-3.

1080 13. Deng, J., Tan, L.H., Kohanski, M.A., Kennedy, D.W., Bosso, J.V., Adappa, N.D.,
1081 Palmer, J.N., Shi, J., and Cohen, N.A. (2021). Solitary chemosensory cells are
1082 innervated by trigeminal nerve endings and autoregulated by cholinergic receptors.
1083 Int Forum Allergy Rhinol *11*, 877–884. 10.1002/alr.22695.

1084 14. Tizzano, M., Gulbransen, B.D., Vandenbeuch, A., Clapp, T.R., Herman, J.P.,
1085 Sibhatu, H.M., Churchill, M.E.A., Silver, W.L., Kinnamon, S.C., and Finger, T.E.
1086 (2010). Nasal chemosensory cells use bitter taste signaling to detect irritants and
1087 bacterial signals. Proc Natl Acad Sci U S A *107*, 3210–3215.
1088 10.1073/pnas.0911934107.

1089 15. Saunders, C.J., Christensen, M., Finger, T.E., and Tizzano, M. (2014).
1090 Cholinergic neurotransmission links solitary chemosensory cells to nasal
1091 inflammation. Proc Natl Acad Sci U S A *111*, 6075–6080. 10.1073/pnas.1402251111.

1092 16. Krasteva, G., Canning, B.J., Hartmann, P., Veres, T.Z., Papadakis, T., Mühlfeld,
1093 C., Schliecker, K., Tallini, Y.N., Braun, A., Hackstein, H., et al. (2011). Cholinergic
1094 chemosensory cells in the trachea regulate breathing. Proc Natl Acad Sci U S A *108*,
1095 9478–9483. 10.1073/pnas.1019418108.

1096 17. Hollenhorst, M.I., Jurastow, I., Nandigama, R., Appenzeller, S., Li, L., Vogel, J.,
1097 Wiederhold, S., Althaus, M., Empting, M., Altmüller, J., et al. (2020). Tracheal brush
1098 cells release acetylcholine in response to bitter tastants for paracrine and autocrine
1099 signaling. FASEB J *34*, 316–332. 10.1096/fj.201901314RR.

1100 18. Lips, K.S., Wunsch, J., Zarghooni, S., Bschleipfer, T., Schukowski, K., Weidner,
1101 W., Wessler, I., Schwantes, U., Koepsell, H., and Kummer, W. (2007). Acetylcholine
1102 and molecular components of its synthesis and release machinery in the urothelium.
1103 Eur Urol *51*, 1042–1053. 10.1016/j.eururo.2006.10.028.

1104 19. Deckmann, K., Filipski, K., Krasteva-Christ, G., Fronius, M., Althaus, M., Rafiq,
1105 A., Papadakis, T., Renno, L., Jurastow, I., Wessels, L., et al. (2014). Bitter triggers
1106 acetylcholine release from polymodal urethral chemosensory cells and bladder
1107 reflexes. Proc Natl Acad Sci U S A *111*, 8287–8292. 10.1073/pnas.1402436111.

1108 20. Gerbe, F., Sidot, E., Smyth, D.J., Ohmoto, M., Matsumoto, I., Dardalhon, V.,
1109 Cesses, P., Garnier, L., Pouzolles, M., Brulin, B., et al. (2016). Intestinal epithelial tuft
1110 cells initiate type 2 mucosal immunity to helminth parasites. Nature *529*, 226–230.
1111 10.1038/nature16527.

1112 21. von Moltke, J., Ji, M., Liang, H.-E., and Locksley, R.M. (2016). Tuft-cell-derived
1113 IL-25 regulates an intestinal ILC2-epithelial response circuit. Nature *529*, 221–225.
1114 10.1038/nature16161.

1115 22. Howitt, M.R., Lavoie, S., Michaud, M., Blum, A.M., Tran, S.V., Weinstock, J.V.,
1116 Gallini, C.A., Redding, K., Margolskee, R.F., Osborne, L.C., et al. (2016). Tuft cells,
1117 taste-chemosensory cells, orchestrate parasite type 2 immunity in the gut. Science
1118 *351*, 1329–1333. 10.1126/science.aaf1648.

1119 23. Schneider, C., O'Leary, C.E., von Moltke, J., Liang, H.-E., Ang, Q.Y., Turnbaugh,
1120 P.J., Radhakrishnan, S., Pellizzon, M., Ma, A., and Locksley, R.M. (2018). A
1121 Metabolite-Triggered Tuft Cell-ILC2 Circuit Drives Small Intestinal Remodeling. Cell
1122 *174*, 271-284.e14. 10.1016/j.cell.2018.05.014.

1123 24. Lei, W., Ren, W., Ohmoto, M., Urban, J.F., Matsumoto, I., Margolskee, R.F., and
1124 Jiang, P. (2018). Activation of intestinal tuft cell-expressed Sucnr1 triggers type 2
1125 immunity in the mouse small intestine. Proc Natl Acad Sci U S A *115*, 5552–5557.
1126 10.1073/pnas.1720758115.

1127 25. Hofmann, T., Chubanov, V., Gudermann, T., and Montell, C. (2003). TRPM5 is a
1128 voltage-modulated and Ca(2+)-activated monovalent selective cation channel. Curr
1129 Biol *13*, 1153–1158. 10.1016/s0960-9822(03)00431-7.

1130 26. O'Leary, C.E., Schneider, C., and Locksley, R.M. (2019). Tuft Cells-Systemically
1131 Dispersed Sensory Epithelia Integrating Immune and Neural Circuitry. Annu Rev
1132 Immunol *37*, 47–72. 10.1146/annurev-immunol-042718-041505.

1133 27. McGinty, J.W., Ting, H.-A., Billipp, T.E., Nadjsombati, M.S., Khan, D.M., Barrett,
1134 N.A., Liang, H.-E., Matsumoto, I., and von Moltke, J. (2020). Tuft-Cell-Derived
1135 Leukotrienes Drive Rapid Anti-helminth Immunity in the Small Intestine but Are
1136 Dispensable for Anti-protist Immunity. Immunity *52*, 528-541.e7.
1137 10.1016/j.immuni.2020.02.005.

1138 28. Marillier, R.G., Michels, C., Smith, E.M., Fick, L.C.E., Leeto, M., Dewals, B.,
1139 Horsnell, W.G.C., and Brombacher, F. (2008). IL-4/IL-13 independent goblet cell
1140 hyperplasia in experimental helminth infections. BMC Immunol *9*, 11. 10.1186/1471-
1141 2172-9-11.

1142 29. McKenzie, G.J., Bancroft, A., Grencis, R.K., and McKenzie, A.N. (1998). A
1143 distinct role for interleukin-13 in Th2-cell-mediated immune responses. Curr Biol *8*,
1144 339–342. 10.1016/s0960-9822(98)70134-4.

1145 30. Miller, H.R., Huntley, J.F., and Wallace, G.R. (1981). Immune exclusion and
1146 mucus trapping during the rapid expulsion of Nippostrongylus brasiliensis from
1147 primed rats. Immunology *44*, 419–429.

1148 31. Grencis, R.K. (2015). Immunity to Helminths: Resistance, Regulation, and
1149 Susceptibility to Gastrointestinal Nematodes. Annual Review of Immunology *33*, 201–
1150 225. 10.1146/annurev-immunol-032713-120218.

1151 32. Oeser, K., Schwartz, C., and Voehringer, D. (2015). Conditional IL-4/IL-13-
1152 deficient mice reveal a critical role of innate immune cells for protective immunity

1153 against gastrointestinal helminths. Mucosal Immunol *8*, 672–682.
1154 10.1038/mi.2014.101.

1155 33. Herbert, D.R., Yang, J.-Q., Hogan, S.P., Groschwitz, K., Khodoun, M., Munitz, A.,
1156 Orekov, T., Perkins, C., Wang, Q., Brombacher, F., et al. (2009). Intestinal epithelial
1157 cell secretion of RELM-beta protects against gastrointestinal worm infection. J Exp
1158 Med *206*, 2947–2957. 10.1084/jem.20091268.

1159 34. Hu, Z., Zhang, C., Sifuentes-Dominguez, L., Zarek, C.M., Propheter, D.C.,
1160 Kuang, Z., Wang, Y., Pendse, M., Ruhn, K.A., Hassell, B., et al. (2021). Small
1161 proline-rich protein 2A is a gut bactericidal protein deployed during helminth infection.
1162 Science (New York, N.Y.) *374*, eabe6723. 10.1126/science.abe6723.

1163 35. Wu, D., Ahrens, R., Osterfeld, H., Noah, T.K., Groschwitz, K., Foster, P.S.,
1164 Steinbrecher, K.A., Rothenberg, M.E., Shroyer, N.F., Matthaei, K.I., et al. (2011).
1165 Interleukin-13 (IL-13)/IL-13 receptor alpha1 (IL-13Ralpha1) signaling regulates
1166 intestinal epithelial cystic fibrosis transmembrane conductance regulator channel-
1167 dependent Cl- secretion. J Biol Chem *286*, 13357–13369. 10.1074/jbc.M110.214965.

1168 36. Horsnell, W.G.C., Cutler, A.J., Hoving, J.C., Mearns, H., Myburgh, E., Arendse,
1169 B., Finkelman, F.D., Owens, G.K., Erle, D., and Brombacher, F. (2007). Delayed
1170 goblet cell hyperplasia, acetylcholine receptor expression, and worm expulsion in
1171 SMC-specific IL-4Ralpha-deficient mice. PLoS Pathog *3*, e1.
1172 10.1371/journal.ppat.0030001.

1173 37. Akiho, H., Blennerhassett, P., Deng, Y., and Collins, S.M. (2002). Role of IL-4, IL-
1174 13, and STAT6 in inflammation-induced hypercontractility of murine smooth muscle
1175 cells. Am J Physiol Gastrointest Liver Physiol *282*, G226-232.
1176 10.1152/ajpgi.2002.282.2.G226.

1177 38. Zhao, A., McDermott, J., Urban, J.F., Gause, W., Madden, K.B., Yeung, K.A.,
1178 Morris, S.C., Finkelman, F.D., and Shea-Donohue, T. (2003). Dependence of IL-4, IL-
1179 13, and nematode-induced alterations in murine small intestinal smooth muscle
1180 contractility on Stat6 and enteric nerves. J Immunol *171*, 948–954.
1181 10.4049/jimmunol.171.2.948.

1182 39. Darby, M., Schnoeller, C., Vira, A., Culley, F.J., Bobat, S., Logan, E., Kirstein, F.,
1183 Wess, J., Cunningham, A.F., Brombacher, F., et al. (2015). The M3 muscarinic
1184 receptor is required for optimal adaptive immunity to helminth and bacterial infection.
1185 PLoS Pathog *11*, e1004636. 10.1371/journal.ppat.1004636.

1186 40. McLean, L.P., Smith, A., Cheung, L., Urban, J.F., Sun, R., Grinchuk, V., Desai,
1187 N., Zhao, A., Raufman, J.-P., and Shea-Donohue, T. (2016). Type 3 muscarinic
1188 receptors contribute to intestinal mucosal homeostasis and clearance of
1189 Nippostrongylus brasiliensis through induction of TH2 cytokines. Am J Physiol
1190 Gastrointest Liver Physiol *311*, G130-141. 10.1152/ajpgi.00461.2014.

1191 41. Sanderson, B.E., and Ogilvie, B.M. (1971). A study of acetylcholinesterase
1192 throughout the life cycle of Nippostrongylus brasiliensis. Parasitology *62*, 367–373.
1193 10.1017/s0031182000077519.

1194 42. Blackburn, C.C., and Selkirk, M.E. (1992). Characterisation of the secretory
1195 acetylcholinesterases from adult Nippostrongylus brasiliensis. Mol Biochem Parasitol
1196 *53*, 79–88. 10.1016/0166-6851(92)90009-9.

1197 43. Lawrence, C.E., and Pritchard, D.I. (1993). Differential secretion of
1198 acetylcholinesterase and proteases during the development of Heligmosomoides
1199 polygyrus. Int J Parasitol *23*, 309–314. 10.1016/0020-7519(93)90004-i.

1200 44. Nadjsombati, M.S., Niepoth, N., Webeck, L.M., Kennedy, E.A., Jones, D.L.,
1201 Baldridge, M.T., Bendesky, A., and Moltke, J. von (2022). Genetic mapping reveals
1202 Pou2af2-dependent tuning of tuft cell differentiation and intestinal type 2 immunity.
1203 2022.10.19.512785. 10.1101/2022.10.19.512785.

1204 45. von Moltke, J., Ji, M., Liang, H.-E., and Locksley, R.M. (2016). Tuft-cell-derived
1205 IL-25 regulates an intestinal ILC2-epithelial response circuit. Nature *529*, 221–225.
1206 10.1038/nature16161.

1207 46. Specian, R.D., and Neutra, M.R. (1980). Mechanism of rapid mucus secretion in
1208 goblet cells stimulated by acetylcholine. J Cell Biol *85*, 626–640.
1209 10.1083/jcb.85.3.626.

1210 47. Gustafsson, J.K., Ermund, A., Johansson, M.E.V., Schütte, A., Hansson, G.C.,
1211 and Sjövall, H. (2012). An ex vivo method for studying mucus formation, properties,
1212 and thickness in human colonic biopsies and mouse small and large intestinal
1213 explants. Am J Physiol Gastrointest Liver Physiol *302*, G430-438.
1214 10.1152/ajpgi.00405.2011.

1215 48. Stockinger, S., Albers, T., Duerr, C.U., Ménard, S., Pütsep, K., Andersson, M.,
1216 and Hornef, M.W. (2014). Interleukin-13-mediated paneth cell degranulation and
1217 antimicrobial peptide release. J Innate Immun *6*, 530–541. 10.1159/000357644.

1218 49. Hubel, K.A. (1976). Intestinal ion transport: effect of norepinephrine, pilocarpine,
1219 and atropine. Am J Physiol *231*, 252–257. 10.1152/ajplegacy.1976.231.1.252.

1220 50. Banks, M.R., and Farthing, M.J.G. (2002). Fluid and electrolyte transport in the
1221 small intestine. Curr Opin Gastroenterol *18*, 176–181. 10.1097/00001574-
1222 200203000-00004.

1223 51. Clarke, L.L. (2009). A guide to Ussing chamber studies of mouse intestine. Am J
1224 Physiol Gastrointest Liver Physiol *296*, G1151-1166. 10.1152/ajpgi.90649.2008.

1225 52. Browning, J.G., Hardcastle, J., Hardcastle, P.T., and Redfern, J.S. (1978).
1226 Localization of the effect of acetylcholine in regulating intestinal ion transport. J
1227 Physiol *281*, 15–27. 10.1113/jphysiol.1978.sp012406.

1228 53. Geubelle, P., Gilissen, J., Dilly, S., Poma, L., Dupuis, N., Laschet, C., Abboud,
1229 D., Inoue, A., Jouret, F., Pirotte, B., et al. (2017). Identification and pharmacological
1230 characterization of succinate receptor agonists. Br J Pharmacol *174*, 796–808.
1231 10.1111/bph.13738.

1232 54. Vanoye, C.G., Altenberg, G.A., and Reuss, L. (1999). Inhibition of P-glycoprotein-
1233 mediated transport by a hydrophobic contaminant in commercial gluconate salts. Am
1234 J Physiol *276*, C1439-1442. 10.1152/ajpcell.1999.276.6.C1439.

1235 55. Harrington, A.M., Hutson, J.M., and Southwell, B.R. (2010). Cholinergic
1236 neurotransmission and muscarinic receptors in the enteric nervous system. Prog
1237 Histochem Cytochem *44*, 173–202. 10.1016/j.proghi.2009.10.001.

1238 56. Xiong, Z., Zhu, X., Geng, J., Xu, Y., Wu, R., Li, C., Fan, D., Qin, X., Du, Y., Tian,
1239 Y., et al. (2022). Intestinal Tuft-2 cells exert antimicrobial immunity via sensing
1240 bacterial metabolite N-undecanoylglycine. Immunity *55*, 686-700.e7.
1241 10.1016/j.immuni.2022.03.001.

1242 57. Keshavarz, M., Faraj Tabrizi, S., Ruppert, A.-L., Pfeil, U., Schreiber, Y., Klein, J.,
1243 Brandenburger, I., Lochnit, G., Bhushan, S., Perniss, A., et al. (2022). Cysteinyl
1244 leukotrienes and acetylcholine are biliary tuft cell cotransmitters. Sci Immunol *7*,
1245 eabf6734. 10.1126/sciimmunol.abf6734.

1246 58. Lee, R.J., Kofonow, J.M., Rosen, P.L., Siebert, A.P., Chen, B., Doghramji, L.,
1247 Xiong, G., Adappa, N.D., Palmer, J.N., Kennedy, D.W., et al. (2014). Bitter and sweet
1248 taste receptors regulate human upper respiratory innate immunity. J. Clin. Invest.
1249 *124*, 1393–1405. 10.1172/JCI72094.

1250 59. Zhu, H., Aryal, D.K., Olsen, R.H.J., Urban, D.J., Swearingen, A., Forbes, S.,
1251 Roth, B.L., and Hochgeschwender, U. (2016). Cre-dependent DREADD (Designer
1252 Receptors Exclusively Activated by Designer Drugs) mice. Genesis *54*, 439–446.
1253 10.1002/dvg.22949.

1254 60. Chen, X., Choo, H., Huang, X.-P., Yang, X., Stone, O., Roth, B.L., and Jin, J.
1255 (2015). The first structure-activity relationship studies for designer receptors
1256 exclusively activated by designer drugs. ACS Chem Neurosci *6*, 476–484.
1257 10.1021/cn500325v.

1258 61. Barilli, A., Aldegheri, L., Bianchi, F., Brault, L., Brodbeck, D., Castelletti, L.,
1259 Feriani, A., Lingard, I., Myers, R., Nola, S., et al. (2021). From High-Throughput
1260 Screening to Target Validation: Benzo[d]isothiazoles as Potent and Selective
1261 Agonists of Human Transient Receptor Potential Cation Channel Subfamily M
1262 Member 5 Possessing In Vivo Gastrointestinal Prokinetic Activity in Rodents. J Med
1263 Chem *64*, 5931–5955. 10.1021/acs.jmedchem.1c00065.

1264 62. Virginio, C., Aldegheri, L., Nola, S., Brodbeck, D., Brault, L., Raveglia, L.F.,
1265 Barilli, A., Sabat, M., and Myers, R. (2022). Identification of positive modulators of

1266 TRPM5 channel from a high-throughput screen using a fluorescent membrane
1267 potential assay. SLAS Discov *27*, 55–64. 10.1016/j.slasd.2021.10.004.

1268 63. Wyatt, K.D., Sakamoto, K., and Watford, W.T. (2022). Tamoxifen administration
1269 induces histopathologic changes within the lungs of Cre-recombinase-negative mice:
1270 A case report. Lab Anim *56*, 297–303. 10.1177/00236772211042968.

1271 64. Chu, C., Parkhurst, C.N., Zhang, W., Zhou, L., Yano, H., Arifuzzaman, M., and
1272 Artis, D. (2021). The ChAT-acetylcholine pathway promotes group 2 innate lymphoid
1273 cell responses and anti-helminth immunity. Sci Immunol *6*, eabe3218.
1274 10.1126/sciimmunol.abe3218.

1275 65. Roberts, L.B., Schnoeller, C., Berkachy, R., Darby, M., Pillaye, J., Oudhoff, M.J.,
1276 Parmar, N., Mackowiak, C., Sedda, D., Quesniaux, V., et al. (2021). Acetylcholine
1277 production by group 2 innate lymphoid cells promotes mucosal immunity to
1278 helminths. Sci Immunol *6*, eabd0359. 10.1126/sciimmunol.abd0359.

1279 66. C, S., Dj, T., and Rk, G. (2018). A sticky end for gastrointestinal helminths; the
1280 role of the mucus barrier. Parasite immunology *40*. 10.1111/pim.12517.

1281 67. Middelhoff, M., Nienhüser, H., Valenti, G., Maurer, H.C., Hayakawa, Y.,
1282 Takahashi, R., Kim, W., Jiang, Z., Malagola, E., Cuti, K., et al. (2020). Prox1-positive
1283 cells monitor and sustain the murine intestinal epithelial cholinergic niche. Nat
1284 Commun *11*, 111. 10.1038/s41467-019-13850-7.

1285 68. Takahashi, T., Shiraishi, A., Murata, J., Matsubara, S., Nakaoka, S., Kirimoto, S.,
1286 and Osawa, M. (2021). Muscarinic receptor M3 contributes to intestinal stem cell
1287 maintenance via EphB/ephrin-B signaling. Life Sci Alliance *4*, e202000962.
1288 10.26508/lsa.202000962.

1289 69. Madden, K.B., Yeung, K.A., Zhao, A., Gause, W.C., Finkelman, F.D., Katona,
1290 I.M., Urban, J.F., and Shea-Donohue, T. (2004). Enteric nematodes induce
1291 stereotypic STAT6-dependent alterations in intestinal epithelial cell function. J
1292 Immunol *172*, 5616–5621. 10.4049/jimmunol.172.9.5616.

1293 70. Schütz, B., Jurastow, I., Bader, S., Ringer, C., von Engelhardt, J., Chubanov, V.,
1294 Gudermann, T., Diener, M., Kummer, W., Krasteva-Christ, G., et al. (2015). Chemical
1295 coding and chemosensory properties of cholinergic brush cells in the mouse
1296 gastrointestinal and biliary tract. Front Physiol *6*, 87. 10.3389/fphys.2015.00087.

1297 71. Jk, G., A, E., D, A., Me, J., He, N., K, T., H, H., H, S., and Gc, H. (2012).
1298 Bicarbonate and functional CFTR channel are required for proper mucin secretion
1299 and link cystic fibrosis with its mucus phenotype. The Journal of experimental
1300 medicine *209*. 10.1084/jem.20120562.

1301 72. Birchenough, G.M.H., Johansson, M.E.V., Gustafsson, J.K., Bergström, J.H., and
1302 Hansson, G.C. (2015). New developments in goblet cell mucus secretion and
1303 function. Mucosal Immunol *8*, 712–719. 10.1038/mi.2015.32.

1304 73. Knoop, K.A., McDonald, K.G., McCrate, S., McDole, J.R., and Newberry, R.D.
1305 (2015). Microbial sensing by goblet cells controls immune surveillance of luminal
1306 antigens in the colon. Mucosal Immunol *8*, 198–210. 10.1038/mi.2014.58.

1307 74. Gustafsson, J.K., Davis, J.E., Rappai, T., McDonald, K.G., Kulkarni, D.H., Knoop,
1308 K.A., Hogan, S.P., Fitzpatrick, J.A., Lencer, W.I., and Newberry, R.D. (2021).
1309 Intestinal goblet cells sample and deliver lumenal antigens by regulated endocytic
1310 uptake and transcytosis. Elife *10*, e67292. 10.7554/eLife.67292.

1311 75. Dolan, B., Ermund, A., Martinez-Abad, B., Johansson, M.E.V., and Hansson,
1312 G.C. (2022). Clearance of small intestinal crypts involves goblet cell mucus secretion
1313 by intracellular granule rupture and enterocyte ion transport. Sci Signal *15*, eabl5848.
1314 10.1126/scisignal.abl5848.

1315 76. Birchenough, G.M.H., Nyström, E.E.L., Johansson, M.E.V., and Hansson, G.C.
1316 (2016). A sentinel goblet cell guards the colonic crypt by triggering Nlrp6-dependent
1317 Muc2 secretion. Science *352*, 1535–1542. 10.1126/science.aaf7419.

1318 77. Morroni, M., Cangiotti, A.M., and Cinti, S. (2007). Brush cells in the human
1319 duodenojejunal junction: an ultrastructural study. J Anat *211*, 125–131.
1320 10.1111/j.1469-7580.2007.00738.x.

1321 78. Cheng, X., Voss, U., and Ekblad, E. (2018). Tuft cells: Distribution and
1322 connections with nerves and endocrine cells in mouse intestine. Exp Cell Res *369*,
1323 105–111. 10.1016/j.yexcr.2018.05.011.

1324 79. Hollenhorst, M.I., Kumar, P., Zimmer, M., Salah, A., Maxeiner, S., Elhawy, M.I.,
1325 Evers, S.B., Flockerzi, V., Gudermann, T., Chubanov, V., et al. (2022). Taste
1326 Receptor Activation in Tracheal Brush Cells by Denatonium Modulates ENaC
1327 Channels via Ca2+, cAMP and ACh. Cells *11*, 2411. 10.3390/cells11152411.

1328 80. Banerjee, A., Herring, C.A., Chen, B., Kim, H., Simmons, A.J., Southard-Smith,
1329 A.N., Allaman, M.M., White, J.R., Macedonia, M.C., Mckinley, E.T., et al. (2020).
1330 Succinate Produced by Intestinal Microbes Promotes Specification of Tuft Cells to
1331 Suppress Ileal Inflammation. Gastroenterology *159*, 2101-2115.e5.
1332 10.1053/j.gastro.2020.08.029.

1333 81. Huh, W.J., Roland, J.T., Asai, M., and Kaji, I. (2020). Distribution of duodenal tuft
1334 cells is altered in pediatric patients with acute and chronic enteropathy. Biomedical
1335 Research *41*, 113–118. 10.2220/biomedres.41.113.

1336 82. Aigbologa, J., Connolly, M., Buckley, J.M., and O'Malley, D. (2020). Mucosal Tuft
1337 Cell Density Is Increased in Diarrhea-Predominant Irritable Bowel Syndrome Colonic
1338 Biopsies. Front Psychiatry *11*, 436. 10.3389/fpsyt.2020.00436.

1339 83. Fung, C., Fraser, L.M., Barrón, G.M., Gologorsky, M.B., Atkinson, S.N., Gerrick,
1340 E.R., Hayward, M., Ziegelbauer, J., Li, J.A., Nico, K.F., et al. (2022). Tuft cells

1341 mediate commensal remodeling of the small intestinal antimicrobial landscape.
1342 2022.10.24.512770. 10.1101/2022.10.24.512770.

1343 84. Sa, R., C, L., Am, M., K, L., Kl, T., C, B., S, K., Sk, G., A, N., Jm, A.-G., et al.
1344 (2019). CFTR-PTEN-dependent mitochondrial metabolic dysfunction promotes
1345 Pseudomonas aeruginosa airway infection. Science translational medicine *11*.
1346 10.1126/scitranslmed.aav4634.

1347 85. Voehringer, D., Reese, T.A., Huang, X., Shinkai, K., and Locksley, R.M. (2006).
1348 Type 2 immunity is controlled by IL-4/IL-13 expression in hematopoietic non-
1349 eosinophil cells of the innate immune system. J Exp Med *203*, 1435–1446.
1350 10.1084/jem.20052448.

1351 86. Me, K., Cm, M., Jg, G., Sd, P., An, G., R, A., S, Y., Pe, B., Ca, S., Pl, Z., et al.
1352 (2022). IL-13-programmed airway tuft cells produce PGE2, which promotes CFTR-
1353 dependent mucociliary function. JCI insight *7*. 10.1172/jci.insight.159832.

1354 87. Nadjsombati, M.S., McGinty, J.W., Lyons-Cohen, M.R., Jaffe, J.B., DiPeso, L.,
1355 Schneider, C., Miller, C.N., Pollack, J.L., Nagana Gowda, G.A., Fontana, M.F., et al.
1356 (2018). Detection of Succinate by Intestinal Tuft Cells Triggers a Type 2 Innate
1357 Immune Circuit. Immunity *49*, 33-41.e7. 10.1016/j.immuni.2018.06.016.

1358 88. Chudnovskiy, A., Mortha, A., Kana, V., Kennard, A., Ramirez, J.D., Rahman, A.,
1359 Remark, R., Mogno, I., Ng, R., Gnjatic, S., et al. (2016). Host-Protozoan Interactions
1360 Protect from Mucosal Infections through Activation of the Inflammasome. Cell *167*,
1361 444-456.e14. 10.1016/j.cell.2016.08.076.

1362 89. Law, C.W., Chen, Y., Shi, W., and Smyth, G.K. (2014). voom: Precision weights
1363 unlock linear model analysis tools for RNA-seq read counts. Genome Biol *15*, R29.
1364 10.1186/gb-2014-15-2-r29.

1365 90. Robinson, M.D., and Oshlack, A. (2010). A scaling normalization method for
1366 differential expression analysis of RNA-seq data. Genome Biol *11*, R25. 10.1186/gb-
1367 2010-11-3-r25.

1368 91. Robinson, M.D., McCarthy, D.J., and Smyth, G.K. (2010). edgeR: a Bioconductor
1369 package for differential expression analysis of digital gene expression data.
1370 Bioinformatics *26*, 139–140. 10.1093/bioinformatics/btp616.

1371 92. Ritchie, M.E., Phipson, B., Wu, D., Hu, Y., Law, C.W., Shi, W., and Smyth, G.K.
1372 (2015). limma powers differential expression analyses for RNA-sequencing and
1373 microarray studies. Nucleic Acids Res *43*, e47. 10.1093/nar/gkv007.

1374